TIME REVERSAL REFOCUSING FOR POINT SOURCE IN RANDOMLY LAYERED MEDIA*

JEAN-PIERRE FOUQUE†, JOSSELIN GARNIER‡, ANDRÉ NACHBIN§, AND KNUT SØLNA¶

Abstract. This paper demonstrates the interest of a time-reversal method for the identification of source in a randomly layered medium. An active source located inside the medium emits a pulse that is recorded on a small time-reversal mirror. The wave is sent back into the medium, either numerically in a computer with the knowledge of the medium, or physically into the real medium. Our goal is to give a precise description of the refocusing of the pulse. We identify and analyze a regime where the pulse refocuses on a ring at the depth of the source and at a critical time. Our objective is to find the location of the source and we show that the time-reveresal refocusing contains information which can be used to this effect and which cannot be obtained by a direct arrival-time analysis. The time reversal technique gives a robust procedure to locate and characterize the source also in the case with ambient noise created by other sources located at the surface.

Key words. Acoustic waves, random media, asymptotic theory, time reversal.

AMS subject classifications. 76B15, 35Q99, 60F05.

1. Introduction.

In the regime of separation of scales a framework for analysis of acoustic waves propagating in randomly layered media has been set forth in [1]. The scale regime we consider corresponds to wavelengths that are large relative to the correlation length of the medium, but short relative to the depth of the source, moreover, we allow the random medium to have strong fluctuations. Here, we first generalize this framework to the case with a source inside of the medium. We then use this approach to implement time reversal and analyze the refocusing properties of the wave field. Time-reversal refocusing for waves propagating in inhomogeneous media has been recently observed and studied experimentally in various contexts, e.g. ultrasound, underwater acoustics, see for instance the review [11]. Important potential applications have been proposed in various fields, for instance imaging [19, 12] and communication [10]. A time-reversal mirror is, roughly speaking, a device which is capable of receiving a signal in time, keeping it in memory and sending it back into the medium in the reversed direction of time. The main effect is the refocusing of the scattered signal after time-reversal in a random medium. Surprisingly, the refocused pulse shape only depends on the statistical properties of the random medium, and not on the particular realization of the medium. The full mathematical understanding, meaning both modeling of the physical problem and derivation of the time-reversal effect, is a complex problem. The study of the one-dimensional case is now well understood [9, 21, 13] as well as the three-dimensional waves in the parabolic or paraxial regime [2, 4, 17].

Our analysis shows how time reversal techniques can be useful for source estimation in the context of randomly layered media. We consider linear acoustic waves

*This work was supported by ONR grants N00014-02-1-0089, N00014-02-1-0603.

†Department of Mathematics, North Carolina State University, Raleigh NC 27695-8205, fouque@math.ncsu.edu

‡Laboratoire de Statistique et Probabilités, Université Paul Sabatier, 118 Route de Narbonne, 31062 Toulouse Cedex 4, France, garnier@cict.fr

§Instituto de Matemática Pura e Aplicade, Est. D Castorina 110, Jardim Botânico, Rio de Janeiro, RJ 22460-320, Brazil, nachbin@impa.br

¶Department of Mathematics, University of California, Irvine CA 92697, ksolna@math.uci.edu

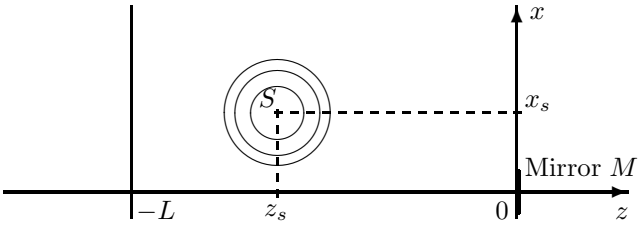

FIG. 1.1. *Emission from a point source.*

propagating in three spatial dimensions:

$$\rho \frac{\partial \mathbf{u}}{\partial t} + \nabla p = \mathbf{F} \tag{1.1}$$

$$\frac{1}{K}\frac{\partial p}{\partial t} + \nabla . \mathbf{u} = 0 \tag{1.2}$$

where p is the pressure, $\mathbf{u}$ is the velocity, ρ is the density of the medium and K the bulk modulus. The forcing term $\mathbf{F}$ is due to the source. In order to simplify the analysis we consider the case with a constant density and a randomly fluctuating bulk modulus which is z-dependent only in the slab $(0, L)$. Note that we choose L so large that the termination of the slab does not affect the wave field at the surface $z = 0$ over the time period that we consider.

$$\rho \equiv \rho_0 \tag{1.3}$$

$$\frac{1}{K} = \begin{cases} \frac{1}{K_0}\left(1 + \nu(\frac{z}{\varepsilon^2})\right) & \text{if } -L < z < 0 \\ \frac{1}{K_0} & \text{if } z > 0 \text{ and } z < -L \end{cases} \tag{1.4}$$

where ν is a zero-mean mixing process and ε^2 is a small dimensionless parameter that characterizes the ratio between the correlation length of the medium and the typical depth of the source. The average velocity is given by $c_0 = \sqrt{K_0/\rho_0}$. A point source located at $(\mathbf{x}_s, z_s)$, $z_s \leq 0$, generates a forcing term $\mathbf{F}$ at time t_s given by:

$$\mathbf{F}(t, x, y, z) = \begin{pmatrix} \mathbf{f_x} \\ f_z \end{pmatrix} (\frac{t - t_s}{\varepsilon})\delta(\mathbf{x} - \mathbf{x}_s)\delta(z - z_s) \tag{1.5}$$

Note that the time duration of the source is short and scaled by ε which is large compared to the correlation length of the medium which is $\mathcal{O}(\varepsilon^2)$. In our time reversal setup we locate a time reversal mirror of spatial size $\mathcal{O}(\varepsilon)$ at the origin. Our setup is illustrated by the cartoon given in Figure 1.1.

In Section 2 we derive an integral representation for the time reversed wave field. The integral representation is obtained by taking a Fourier transform in the time and lateral space coordinates. This reduces the problem to a family of one dimensional problems that can be analyzed by decomposing the wave field into right and left going waves. In Section 3 we consider the particular case where the source is at the surface ($z_s = 0$). We carry out a careful stationary phase analysis combined with classic diffusion approximation results in the limit of small ε. This gives a limit with explicit formulas for the time reversed wave field which reveal a refocusing of the pulse at a critical time at the surface $z = 0$ and on a circle centered at the time reversal mirror and passing through the source. If the time reversal mirror only has point support

the refocusing is uniform on the circle, while a small spatial extent mirror enables estimation of the angle to the source. In Section 4 we consider the important case with an internal source, also in this case we are able to carry out the asymptotic analysis that characterizes the limiting time reversed wave field. Even though the formulas are not explicit in this case we can still deduce the refocusing of the wave field and that it happens at a critical time, at the depth of the source and on a circle as in the previous case. In Section 5 we discuss a possible application to the problem of the source location and identification. In Section 6 we present a set of numerical experiments which illustrate the results obtained in this paper.

2. The Time Reversed Wave Field.

2.1. Emission from a point source. In the scaling that we consider the typical wavelength of the source is small $\mathcal{O}(\varepsilon)$ and we use the following specific Fourier transform and its inverse with respect to time and the transverse direction:

$$\hat{p}(\omega,\boldsymbol{\kappa},z)=\int\int p(t,\mathbf{x},z)e^{i\frac{\omega}{\varepsilon}(t-\boldsymbol{\kappa}.\mathbf{x})}dtd\mathbf{x}$$

$$p(t,\mathbf{x},z)=\frac{1}{(2\pi\varepsilon)^3}\int\int\hat{p}(\omega,\boldsymbol{\kappa},z)e^{-i\frac{\omega}{\varepsilon}(t-\boldsymbol{\kappa}.\mathbf{x})}\omega^2 d\omega d\boldsymbol{\kappa}$$

where $\mathbf{x}=(x,y)$ stands for the transverse spatial variables. Taking the scaled Fourier transform gives that $\hat{\mathbf{u}}=(\hat{\mathbf{v}},\hat{u})$ and $\hat{p}$ satisfy the system:

$$-\rho_0\frac{i\omega}{\varepsilon}\hat{\mathbf{v}}+i\frac{\omega}{\varepsilon}\boldsymbol{\kappa}\hat{p}=\varepsilon\hat{\mathbf{f}}_{\mathbf{x}}(\omega)e^{i\frac{\omega}{\varepsilon}(t_s-\boldsymbol{\kappa}.\mathbf{x}_s)}\delta(z-z_s) \tag{2.1}$$

$$-\rho_0\frac{i\omega}{\varepsilon}\hat{u}+\frac{\partial\hat{p}}{\partial z}=\varepsilon\hat{f}_z(\omega)e^{i\frac{\omega}{\varepsilon}(t_s-\boldsymbol{\kappa}.\mathbf{x}_s)}\delta(z-z_s) \tag{2.2}$$

$$-\frac{1}{K(z)}\frac{i\omega}{\varepsilon}\hat{p}+i\frac{\omega}{\varepsilon}\boldsymbol{\kappa}.\hat{\mathbf{v}}+\frac{\partial\hat{u}}{\partial z}=0 \tag{2.3}$$

where $\hat{f}$ is the ordinary unscaled Fourier transform of the pulse profile

$$\hat{f}(\omega)=\int f(t)e^{i\omega t}dt,\qquad f(t)=\frac{1}{2\pi}\int\hat{f}(\omega)e^{-i\omega t}d\omega$$

We deduce that $(\hat{u},\hat{p})$ satisfy the following closed system for $-L<z<z_s$ and $z_s<z<0$

$$\frac{\partial\hat{u}}{\partial z}+\frac{i\omega}{\varepsilon}\left(-\frac{1}{K(z)}+\frac{|\boldsymbol{\kappa}|^2}{\rho_0}\right)\hat{p}=0 \tag{2.4}$$

$$\frac{\partial\hat{p}}{\partial z}-\frac{i\omega}{\varepsilon}\rho_0\hat{u}=0 \tag{2.5}$$

with the jumps at $z=z_s$ given by

$$[\hat{u}]_{z_s}=\varepsilon\frac{\boldsymbol{\kappa}.\hat{\mathbf{f}}_{\mathbf{x}}(\omega)}{\rho_0}e^{i\frac{\omega}{\varepsilon}(t_s-\boldsymbol{\kappa}.\mathbf{x}_s)} \tag{2.6}$$

$$[\hat{p}]_{z_s}=\varepsilon\hat{f}_z(\omega)e^{i\frac{\omega}{\varepsilon}(t_s-\boldsymbol{\kappa}.\mathbf{x}_s)} \tag{2.7}$$

We introduce the right and left propagating wave modes a and b which are defined by

$$\hat{p}(\omega,\boldsymbol{\kappa},z)=\frac{\sqrt{I_0(\kappa)}}{2}\left(a(\omega,\boldsymbol{\kappa},z)e^{i\frac{\omega}{\varepsilon}\zeta_0(\kappa)z}-b(\omega,\boldsymbol{\kappa},z)e^{-i\frac{\omega}{\varepsilon}\zeta_0(\kappa)z}\right) \tag{2.8}$$

$$\hat{u}(\omega,\boldsymbol{\kappa},z)=\frac{1}{2\sqrt{I_0(\kappa)}}\left(a(\omega,\boldsymbol{\kappa},z)e^{i\frac{\omega}{\varepsilon}\zeta_0(\kappa)z}+b(\omega,\boldsymbol{\kappa},z)e^{-i\frac{\omega}{\varepsilon}\zeta_0(\kappa)z}\right) \tag{2.9}$$

where $\kappa = |\boldsymbol{\kappa}|$, $\zeta_0^{-1}(\kappa)$ is the average longitudinal velocity, and $I_0(\kappa)$ is the acoustic impedance

$$\zeta_0(\kappa) = \frac{\sqrt{1 - c_0^2\kappa^2}}{c_0}, \qquad I_0(\kappa) = \frac{\rho_0}{\zeta_0(\kappa)}.$$

Here we only consider propagating modes and ignore evanescent modes meaning that $|\kappa| < c_0^{-1}$. The system for a and b can be written as

$$\frac{\partial}{\partial z}\begin{pmatrix} a \\ b \end{pmatrix}(\omega,\kappa,z) = Q^\varepsilon(\omega,\kappa,z)\begin{pmatrix} a \\ b \end{pmatrix}(\omega,\kappa,z) \tag{2.10}$$

where the complex 2×2 matrix Q^ε is given by

$$Q^\varepsilon(\omega,\kappa,z) = \frac{i\omega\zeta_0(\kappa)}{2\varepsilon}\nu_\kappa(\frac{z}{\varepsilon^2})\begin{pmatrix} 1 & -e^{\frac{-2i\omega\zeta_0(\kappa)z}{\varepsilon}} \\ e^{\frac{2i\omega\zeta_0(\kappa)z}{\varepsilon}} & -1 \end{pmatrix}. \tag{2.11}$$

The mode-dependent random process ν_κ is defined by

$$\nu_\kappa(\frac{z}{\varepsilon^2}) = \frac{1}{1 - c_0^2\kappa^2}\nu(\frac{z}{\varepsilon^2}).$$

Using the definitions (2.8) and (2.9) of a and b and the expressions (2.6) and (2.7) for the jumps in $\hat{u}$ and $\hat{p}$ we deduce the jumps at $z = z_s$ for the modes a and b

$$[a]_{z_s} = \varepsilon e^{i\frac{\omega}{\varepsilon}(t_s - \boldsymbol{\kappa}.\mathbf{x}_s - \zeta_0(\kappa)z_s)}S_a(\omega,\boldsymbol{\kappa}), \tag{2.12}$$

$$[b]_{z_s} = \varepsilon e^{i\frac{\omega}{\varepsilon}(t_s - \boldsymbol{\kappa}.\mathbf{x}_s + \zeta_0(\kappa)z_s)}S_b(\omega,\boldsymbol{\kappa}), \tag{2.13}$$

with the source contributions given by

$$S_a(\omega,\boldsymbol{\kappa}) = \frac{\sqrt{I_0(\kappa)}}{\rho_0}\boldsymbol{\kappa}.\hat{\mathbf{f}}_{\mathbf{x}}(\omega) + \frac{1}{\sqrt{I_0(\kappa)}}\hat{f}_z(\omega) \tag{2.14}$$

$$S_b(\omega,\boldsymbol{\kappa}) = \frac{\sqrt{I_0(\kappa)}}{\rho_0}\boldsymbol{\kappa}.\hat{\mathbf{f}}_{\mathbf{x}}(\omega) - \frac{1}{\sqrt{I_0(\kappa)}}\hat{f}_z(\omega). \tag{2.15}$$

The system for a and b is associated with boundary conditions at $z = 0$ and $z = -L$ that are shown in Figure 2.1. We assume that no energy is coming from $+\infty$ and $-\infty$, so that we get the radiation conditions

$$a(\omega,\boldsymbol{\kappa},-L) = 0, \qquad b(\omega,\boldsymbol{\kappa},0) = 0.$$

The quantity of interest is the wave field at the surface which is completely characterized by $a(\omega,\boldsymbol{\kappa},0)$ since $b(\omega,\boldsymbol{\kappa},0) = 0$.

We transform this boundary value problem into an initial value problem by introducing the propagator $Y(\omega,\kappa,z_0,z)$, $-L \le z_0 \le z \le 0$, which is a family of complex 2×2 matrices solutions of

$$\frac{\partial Y}{\partial z} = Q^\varepsilon(\omega,\kappa,z)Y, \qquad Y(\omega,\kappa,z_0,z = z_0) = \mathrm{Id}_{\mathbb{C}^2}.$$

By using the particular form of the matrix Q^ε in (2.11) one can show that if the column vector $(\alpha,\beta)^T$ is solution of equation (2.10) with the initial conditions

$$\alpha(z_0,z = z_0) = 1, \qquad \beta(z_0,z = z_0) = 0, \tag{2.16}$$

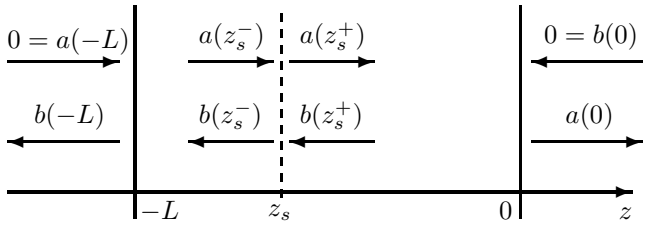

FIG. 2.1. *Boundary conditions at $z = -L$ and $z = 0$ corresponding to the emission from the point source located at depth z_s.*

then the column vector $(\overline{\beta}, \overline{\alpha})^T$ is another solution linearly independent of the first solution, so that the propagator matrix Y can be written as:

$$Y(z_0, z) = \begin{pmatrix} \alpha & \overline{\beta} \\ \beta & \overline{\alpha} \end{pmatrix} (z_0, z).$$

The boundary conditions at $z = -L$ and $z = 0$ then imply

$$Y(-L, z_s) \begin{pmatrix} 0 \\ b(-L) \end{pmatrix} = \begin{pmatrix} a(z_s^-) \\ b(z_s^-) \end{pmatrix} \tag{2.17}$$

$$Y(z_s, 0) \begin{pmatrix} a(z_s^+) \\ b(z_s^+) \end{pmatrix} = \begin{pmatrix} a(0) \\ 0 \end{pmatrix}. \tag{2.18}$$

The system determined by (2.12, 2.13, 2.17, 2.18) whose unknown are $b(-L)$ and $a(0)$ can be solved, and we get

$$\begin{aligned} a(\omega, \boldsymbol{\kappa}, 0) = \varepsilon e^{i\frac{\omega}{\varepsilon}(t_s - \boldsymbol{\kappa}.\mathbf{x}_s)} \Big[& e^{-i\frac{\omega}{\varepsilon}\zeta_0(\kappa) z_s} T_g(\omega, \kappa, z_s) S_a(\omega, \boldsymbol{\kappa}) \\ & - e^{i\frac{\omega}{\varepsilon}\zeta_0(\kappa) z_s} R_g(\omega, \kappa, z_s) S_b(\omega, \boldsymbol{\kappa}) \Big] \end{aligned} \tag{2.19}$$

where R_g and T_g are the coefficients defined by

$$R_g(\omega, \kappa, z) = \frac{\frac{\overline{\beta}}{\overline{\alpha}}(\omega, \kappa, -L, z)}{\overline{\alpha}(\omega, \kappa, z, 0) + \beta(\omega, \kappa, z, 0)\frac{\overline{\beta}}{\overline{\alpha}}(\omega, \kappa, -L, z)} \tag{2.20}$$

$$T_g(\omega, \kappa, z) = \frac{1}{\overline{\alpha}(\omega, \kappa, z, 0) + \beta(\omega, \kappa, z, 0)\frac{\overline{\beta}}{\overline{\alpha}}(\omega, \kappa, -L, z)} \tag{2.21}$$

Observe that these coefficients are generalized versions of those used in [1] as we explain now. The transmission and reflection coefficients $T(\omega, \kappa - L, z)$ and $R(\omega, \kappa, -L, z)$ for a slab $[-L, z]$ (see Figure 2.2) are given in terms of α and β as

$$R(\omega, \kappa, -L, z) = \frac{\overline{\beta}}{\overline{\alpha}}(\omega, \kappa, -L, z), \qquad T(\omega, \kappa, -L, z) = \frac{1}{\overline{\alpha}}(\omega, \kappa, -L, z).$$

We also introduce $\widetilde{R}$ and $\widetilde{T}$ defined as the reflection and transmission coefficients for the experiment corresponding to a right-going input wave incoming from the left (see Figure 2.3). They are given in terms of α and β by

$$\widetilde{R}(\omega, \kappa, z, 0) = -\frac{\beta}{\overline{\alpha}}(\omega, \kappa, z, 0), \qquad \widetilde{T}(\omega, \kappa, z, 0) = \frac{1}{\overline{\alpha}}(\omega, \kappa, z, 0).$$

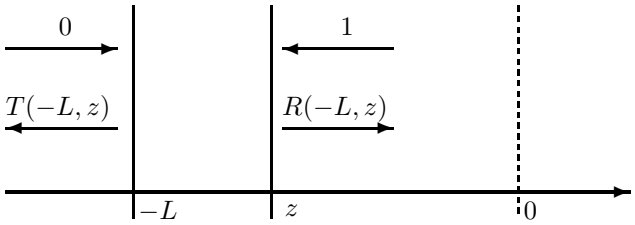

FIG. 2.2. *Reflection and transmission coefficients.*

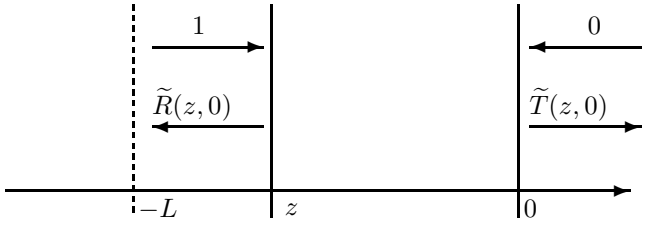

FIG. 2.3. *Adjoint reflection and transmission coefficients.*

We can express the coefficients R_g and T_g in terms of the usual reflection and transmission coefficients R and T for which the asymptotic analysis of the moments has been carried out in [1] and will be used in subsequent sections.

$$R_g(\omega,\kappa,z) = \frac{\widetilde{T}(\omega,\kappa,z,0)R(\omega,\kappa,-L,z)}{1-\widetilde{R}(\omega,\kappa,z,0)R(\omega,\kappa,-L,z)} \tag{2.22}$$

$$T_g(\omega,\kappa,z) = \frac{\widetilde{T}(\omega,\kappa,z,0)}{1-\widetilde{R}(\omega,\kappa,z,0)R(\omega,\kappa,-L,z)} \tag{2.23}$$

We denote the wave at the surface $z=0$ by $(\mathbf{u}_s, p_s)$. We have

$$p_s(t,\mathbf{x}) = \frac{1}{(2\pi\varepsilon)^3}\int \frac{\sqrt{I_0(\kappa)}}{2} a(\omega,\boldsymbol{\kappa},0)e^{-i\frac{\omega}{\varepsilon}(t-\boldsymbol{\kappa}.\mathbf{x})}\omega^2 d\omega d\boldsymbol{\kappa} \tag{2.24}$$

$$u_s(t,\mathbf{x}) = \frac{1}{(2\pi\varepsilon)^3}\int \frac{1}{2\sqrt{I_0(\kappa)}} a(\omega,\boldsymbol{\kappa},0)e^{-i\frac{\omega}{\varepsilon}(t-\boldsymbol{\kappa}.\mathbf{x})}\omega^2 d\omega d\boldsymbol{\kappa} \tag{2.25}$$

$$\mathbf{v}_s(t,\mathbf{x}) = \frac{1}{(2\pi\varepsilon)^3}\int \frac{\sqrt{I_0(\kappa)}}{2\rho_0}\boldsymbol{\kappa} a(\omega,\boldsymbol{\kappa},0)e^{-i\frac{\omega}{\varepsilon}(t-\boldsymbol{\kappa}.\mathbf{x})}\omega^2 d\omega d\boldsymbol{\kappa} \tag{2.26}$$

These signals comprise a coherent front wave of duration $\mathcal{O}(\varepsilon)$ corresponding to the duration of the source, moreover, a long noisy coda part that is caused by the multiple scattering by the layers. These coda waves are a part of, and play a crucial role in, the time reversal procedure that we describe next.

2.2. Recording, time-reversal and reemission. The first step of the time reversal procedure consists in recording the velocity signal at $z=0$ at the mirror $M = \{(\mathbf{x},z), \mathbf{x}\in D^\varepsilon, z=0\}$ during some time interval centered at $t=0$. $D^\varepsilon \subset \mathbb{R}^2$ is the shape of the mirror whose center is located at point $\mathbf{0}$. It turns out that as $\varepsilon \to 0$ the interesting asymptotic regime arises when we record the signal during a large time interval whose duration is of order 1 and is denoted by t_1 with $t_1 > 0$. We consider here the practical situation where the mirror is not very large, but of a size of the order of a few wavelengths (i.e. of order ε).

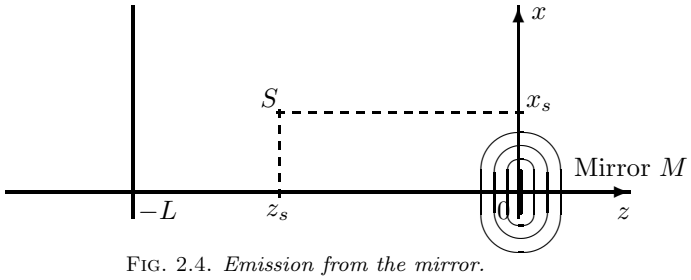

FIG. 2.4. *Emission from the mirror.*

In the second step of the time reversal procedure a piece of the recorded signal is clipped using a cut-off function $s \mapsto G_1(s)$ where the support of G_1 is included in $[-t_1/2, t_1/2]$. We denote the recorded part of the wave by $\mathbf{u}_{rec}$ so that

$$\mathbf{u}_{rec}(t, \mathbf{x}) = \mathbf{u}_s(t, \mathbf{x}) G_1(t) G_2(\frac{\mathbf{x}}{\varepsilon}),$$

where G_2 is the spatial cut-off function introduced by the mirror of typical size ε with

$$G_2(\mathbf{x}) = \mathbf{1}_D(\mathbf{x})$$

and D is the shape of the mirror. We then time reverse this piece of signal and send it back into the same medium as illustrated in Figure 2.4. This means that we address a new problem defined by the acoustic equations (1.1-1.2) with the source term

$$\vec{\mathbf{F}}_{TR}(t, \mathbf{x}, z) = \rho_0 c_0 \mathbf{u}_{rec}(-t, \mathbf{x}) \delta(z)$$

where *TR* stands for "Time Reversal" and the factor $\rho_0 c_0$ has been added to restore the physical dimension of the expression. Note that by linearity of the problem this factor plays no role in the analysis. In terms of right and left-going wave modes, the system consists of the linear system (2.10) for $-L \leq z < 0$, with the boundary conditions,

$$b_{TR}(\omega, \boldsymbol{\kappa}, 0^+) = 0, \qquad a_{TR}(\omega, \boldsymbol{\kappa}, -L) = 0$$

see Figure 2.5, and the jump condition

$$[b_{TR}]_0 = \frac{\sqrt{I_0(\kappa)}}{\rho_0} \boldsymbol{\kappa}.\hat{\mathbf{F}}_{TR,\mathbf{x}}(\omega, \boldsymbol{\kappa}) - \frac{1}{\sqrt{I_0(\kappa)}} \hat{F}_{TR,z}(\omega, \boldsymbol{\kappa})$$

where

$$\hat{\mathbf{F}}_{TR,\mathbf{x}}(\omega, \boldsymbol{\kappa}) = \frac{\rho_0 c_0}{(2\pi)^3 \varepsilon} \int \frac{\sqrt{I_0(\kappa')}}{2\rho_0} \boldsymbol{\kappa}' \overline{a}(\omega', \boldsymbol{\kappa}', 0) \overline{\hat{G}_1}(\frac{\omega - \omega'}{\varepsilon}) \hat{G}_2(\omega \boldsymbol{\kappa} + \omega' \boldsymbol{\kappa}') \omega'^2 d\omega' d\boldsymbol{\kappa}'$$

$$\hat{F}_{TR,z}(\omega, \boldsymbol{\kappa}) = \frac{\rho_0 c_0}{(2\pi)^3 \varepsilon} \int \frac{1}{\sqrt{I_0(\kappa')}} \overline{a}(\omega', \boldsymbol{\kappa}', 0) \overline{\hat{G}_1}(\frac{\omega - \omega'}{\varepsilon}) \hat{G}_2(\omega \boldsymbol{\kappa} + \omega' \boldsymbol{\kappa}') \omega'^2 d\omega' d\boldsymbol{\kappa}'.$$

The quantity $a(\omega, \boldsymbol{\kappa}, 0)$ is given by (2.19), and the Fourier transformed window functions are defined by

$$\hat{G}_1(\omega) = \int G_1(t) e^{i\omega t} dt, \qquad \hat{G}_2(\mathbf{k}) = \int G_2(\mathbf{x}) e^{-i\mathbf{k}.\mathbf{x}} d\mathbf{x}.$$

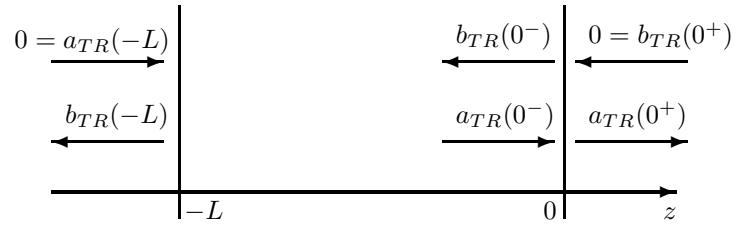

FIG. 2.5. *Boundary conditions at $z = -L$ and $z = 0$ corresponding to the emission from the mirror located at $z = 0$.*

This configuration can then be reduced to the system (2.10) for $-L \le z < 0$. From $b_{TR}(0^-) = -[b_{TR}]_0$ and the expressions for $\hat{\mathbf{F}}_{TR,\mathbf{x}}$ and $\hat{F}_{TR,z}$ given above we deduce the boundary condition at $z = 0$

$$b_{TR}(\omega, \boldsymbol{\kappa}, 0^-) = \frac{1}{(2\pi)^3 \varepsilon} \int \frac{H_0(\boldsymbol{\kappa}, \boldsymbol{\kappa}')}{2} \overline{a}(\omega', \boldsymbol{\kappa}', 0) \overline{\hat{G}_1}(\frac{\omega - \omega'}{\varepsilon}) \hat{G}_2(\omega \boldsymbol{\kappa} + \omega' \boldsymbol{\kappa}') \omega'^2 d\omega' d\boldsymbol{\kappa}'$$

where

$$H_0(\boldsymbol{\kappa}, \boldsymbol{\kappa}') = \frac{\rho_0 c_0}{\sqrt{I_0(\kappa) I_0(\kappa')}} - \frac{\rho_0 c_0 \sqrt{I_0(\kappa) I_0(\kappa')}}{\rho_0^2} \boldsymbol{\kappa}.\boldsymbol{\kappa}'.$$

The boundary at $z = -L$ is simply

$$a_{TR}(\omega, \boldsymbol{\kappa}, -L) = 0.$$

The Fourier transformed pressure and velocity are now given by (2.8) and (2.9) where a and b are replaced by a_{TR} and b_{TR}.

2.3. The time reversed wave field. The new incoming signal propagates into the same medium and produces the time reversed wave field. Here we derive an exact integral representation for this wave field which will be exploited to analyze the refocusing properties of the time reversed field in the following sections. Using once again the propagator we get that the wave for $-L \le z \le 0$ is given by

$$u_{TR}(t, \mathbf{x}, z) = \frac{1}{(2\pi\varepsilon)^3} \int \frac{1}{2\sqrt{I_0(\kappa)}} b_{TR}(\omega, \boldsymbol{\kappa}, 0) \Big[R_g(\omega, \kappa, z) e^{i\frac{\omega}{\varepsilon}\zeta_0(\kappa) z} + T_g(\omega, \kappa, z) e^{-i\frac{\omega}{\varepsilon}\zeta_0(\kappa) z} \Big] e^{-i\frac{\omega}{\varepsilon}(t - \boldsymbol{\kappa}.\mathbf{x})} \omega^2 d\omega d\boldsymbol{\kappa}$$

and similar expressions hold for $p_{TR}(t, \mathbf{x}, z)$ and $\mathbf{v}_{TR}(t, \mathbf{x}, z)$. Substituting the expression of $b_{TR}(\omega, \boldsymbol{\kappa}, 0^-)$ into this equation yields the following representation of the longitudinal velocity

$$u_{TR}(t, \mathbf{x}, z) = \frac{1}{(2\pi)^6 \varepsilon^3} \int \int \frac{H_0(\boldsymbol{\kappa}, \boldsymbol{\kappa}')}{4\sqrt{I_0(\kappa)}} \overline{\hat{G}_1}(\frac{\omega - \omega'}{\varepsilon}) \hat{G}_2(\omega \boldsymbol{\kappa} + \omega' \boldsymbol{\kappa}')$$

$$\times e^{i\left(\frac{-(\omega' t_s + \omega t) + (\omega' \boldsymbol{\kappa}'.\mathbf{x}_s + \omega \boldsymbol{\kappa}.\mathbf{x})}{\varepsilon}\right)} \left[\sum_{j=1}^{4} P_j \right] \omega^2 \omega'^2 d\omega d\boldsymbol{\kappa} d\omega' d\boldsymbol{\kappa}' \tag{2.27}$$

where we define the P_j's by

$$P_1 = -e^{i\left(\frac{-\omega' \zeta_0(\kappa') z_s + \omega \zeta_0(\kappa) z}{\varepsilon}\right)} \overline{R_g}(\omega', \kappa', z_s) R_g(\omega, \kappa, z) \overline{S_b}(\omega', \boldsymbol{\kappa}')$$

$$P_2 = e^{i\left(\frac{\omega'\zeta_0(\kappa')z_s+\omega\zeta_0(\kappa)z}{\varepsilon}\right)}\overline{T_g}(\omega',\kappa',z_s)R_g(\omega,\kappa,z)\overline{S_a}(\omega',\boldsymbol{\kappa}')$$
$$P_3 = e^{i\left(\frac{\omega'\zeta_0(\kappa')z_s-\omega\zeta_0(\kappa)z}{\varepsilon}\right)}\overline{T_g}(\omega',\kappa',z_s)T_g(\omega,\kappa,z)\overline{S_a}(\omega',\boldsymbol{\kappa}')$$
$$P_4 = -e^{i\left(\frac{-\omega'\zeta_0(\kappa')z_s-\omega\zeta_0(\kappa)z}{\varepsilon}\right)}\overline{R_g}(\omega',\kappa',z_s)T_g(\omega,\kappa,z)\overline{S_b}(\omega',\boldsymbol{\kappa}').$$

Motivated by the presence of the term $\bar{\hat{G}}_1(\frac{\omega-\omega'}{\varepsilon})$ we perform the change of variables $\omega' = \omega_c + \varepsilon h/2$, $\omega = \omega_c - \varepsilon h/2$. Due to the fact that the generalized transmission and reflection coefficients only depend on the moduli of the slowness vectors, we use polar coordinates (μ,θ) and (μ',θ') for $\boldsymbol{\kappa} = \mu\mathbf{e}_\theta$ and $\boldsymbol{\kappa}' = \mu'\mathbf{e}_{\theta'}$. We also represent the observation point $\mathbf{x}$ and the source position $\mathbf{x}_s$ by $r_0\mathbf{e}_{\theta_0}$ and $r_s\mathbf{e}_{\theta_s}$, respectively, where we denote by $\mathbf{e}_\theta$ the unit column vector $(\cos(\theta),\sin(\theta))^T$. Finally we get:

$$\begin{aligned} u_{TR}(t,\mathbf{x}=r_0\mathbf{e}_{\theta_0},z) &= \frac{1}{(2\pi)^6\varepsilon^2}\int\int \frac{H_0(\mu\mathbf{e}_\theta,\mu'\mathbf{e}_{\theta'})}{4\sqrt{I_0(\mu)}} \\ &\times\overline{\hat{G}_1}(-h)\hat{G}_2\left((\omega_c-\frac{\varepsilon h}{2})\mu\mathbf{e}_\theta+(\omega_c+\frac{\varepsilon h}{2})\mu'\mathbf{e}_{\theta'}\right) \\ &\times e^{i\frac{\omega_c}{\varepsilon}\left(-(t_s+t)+\mu' r_s\cos(\theta_s-\theta')+\mu r_0\cos(\theta-\theta_0)\right)}e^{i\frac{h}{2}\left(-t_s+t+\mu' r_s\cos(\theta_s-\theta')-\mu r_0\cos(\theta-\theta_0)\right)} \\ &\times\left[\sum_{j=1}^4 P_j\right]\mu\mu'\left(\omega_c^2-\frac{\varepsilon^2h^2}{4}\right)^2 d\omega_c dh d\mu d\mu' d\theta d\theta' \end{aligned} \tag{2.28}$$

with

$$\begin{aligned} P_1 &= -e^{i\frac{\omega_c}{\varepsilon}\left(-\zeta_0(\mu')z_s+\zeta_0(\mu)z\right)}e^{i\frac{h}{2}\left(-\zeta_0(\mu')z_s-\zeta_0(\mu)z\right)} \\ &\quad\times\overline{R_g}(\omega_c+\frac{\varepsilon h}{2},\mu',z_s)R_g(\omega_c-\frac{\varepsilon h}{2},\mu,z)\overline{S_b}(\omega_c+\frac{\varepsilon h}{2},\mu'\mathbf{e}_{\theta'}) \\ P_2 &= e^{i\frac{\omega_c}{\varepsilon}\left(\zeta_0(\mu')z_s+\zeta_0(\mu)z\right)}e^{i\frac{h}{2}\left(\zeta_0(\mu')z_s-\zeta_0(\mu)z\right)} \\ &\quad\times\overline{T_g}(\omega_c+\frac{\varepsilon h}{2},\mu',z_s)R_g(\omega_c-\frac{\varepsilon h}{2},\mu,z)\overline{S_a}(\omega_c+\frac{\varepsilon h}{2},\mu'\mathbf{e}_{\theta'}) \\ P_3 &= e^{i\frac{\omega_c}{\varepsilon}\left(\zeta_0(\mu')z_s-\zeta_0(\mu)z\right)}e^{i\frac{h}{2}\left(\zeta_0(\mu')z_s+\zeta_0(\mu)z\right)} \\ &\quad\times\overline{T_g}(\omega_c+\frac{\varepsilon h}{2},\mu',z_s)T_g(\omega_c-\frac{\varepsilon h}{2},\mu,z)\overline{S_a}(\omega_c+\frac{\varepsilon h}{2},\mu'\mathbf{e}_{\theta'}) \\ P_4 &= -e^{i\frac{\omega_c}{\varepsilon}\left(-\zeta_0(\mu')z_s-\zeta_0(\mu)z\right)}e^{i\frac{h}{2}\left(-\zeta_0(\mu')z_s+\zeta_0(\mu)z\right)} \\ &\quad\times\overline{R_g}(\omega_c+\frac{\varepsilon h}{2},\mu',z_s)T_g(\omega_c-\frac{\varepsilon h}{2},\mu,z)\overline{S_b}(\omega_c+\frac{\varepsilon h}{2},\mu'\mathbf{e}_{\theta'}) \end{aligned}$$

In the following sections we study the asymptotic behavior of the time reversed wave field u_{TR} in the limit $\varepsilon \to 0$. This is done in the particular case where the source is located on the surface ($z_s = 0$) in Section 3, and in the general case where the source is inside of the medium ($z_s < 0$) in Section 4.

3. Exterior point source . In this section we assume that the source is located on the surface $(\mathbf{x}_s, z_s = 0)$. We also observe the time-reversed wave at the surface $(\mathbf{x}, z = 0)$. Under such conditions the generalized transmission and reflection coefficients T_g and R_g are evaluated at $z = 0$ and from their definitions, (2.22) and (2.23), it follows that the transmission coefficient T_g is equal to one, and the reflection coefficient R_g corresponds to the reflections from the whole random medium between $-L$ and the surface, that is to say $R(-L,0)$. The deterministic P_3 term of u_{TR} is

associated with a product of transmission coefficients, it corresponds to recording and reemission of the directly transmitted wave field from the source to the mirror and then observation of the wave field that is directly transmitted back to the source point. The P_2 and P_4 terms are associated with one transmission and one reflection coefficient, they correspond respectively to (i) the wave that is directly transmitted to the mirror, then time reversed, reemitted into the random medium and subsequently scattered back from the random medium and onto the recorder at the source point, (ii) the wave component that is reflected from the random medium onto the mirror then time reversed and transmitted directly back to the recorder at the source point. The P_1 term, the one defined in terms of a product of reflection coefficients, corresponds to the wave which has been scattered back twice by the random medium. From the point of view of refocusing of time reversed waves in a random medium this last term turns out to be the most interesting one.

3.1. Homogeneous medium. We first examine the deterministic case with $\nu \equiv 0$ which corresponds to a homogeneous medium. The time reversed wave field is then described by (2.28) with $R = 0$ and $T = 1$. In this case only the P_3 term in u_{TR} corresponding to direct transmission paths contributes, recall that this component remains unchanged in the the random case with $\nu \neq 0$. The wave emitted from the source that can be observed at the surface consists of pressure and velocity fields. The pressure field in (2.24) for $\mathbf{x} \neq \mathbf{x}_s$ is given by

$$p_s(t,\mathbf{x}) = -\nabla_{\mathbf{x}}.\left[\frac{1}{4\pi|\mathbf{x}-\mathbf{x}_s|}\mathbf{f}_{\mathbf{x}}\left(\frac{t-t_s-\frac{|\mathbf{x}-\mathbf{x}_s|}{c_0}}{\varepsilon}\right)\right],$$

where the evanescent wave has been neglected as they will play no role in our far-field configuration. For small ε the leading order part of the pressure field is given by

$$p_s(t,\mathbf{x}) = \frac{1}{4\pi c_0\varepsilon|\mathbf{x}-\mathbf{x}_s|^2}(\mathbf{x}-\mathbf{x}_s).\mathbf{f}'_{\mathbf{x}}\left(\frac{t-t_s-\frac{|\mathbf{x}-\mathbf{x}_s|}{c_0}}{\varepsilon}\right).$$

Similarly the leading order terms of the longitudinal and transverse velocity fields are

$$u_s(t,\mathbf{x}) = -\frac{1}{4\pi\rho_0 c_0|\mathbf{x}-\mathbf{x}_s|^2}f_z\left(\frac{t-t_s-\frac{|\mathbf{x}-\mathbf{x}_s|}{c_0}}{\varepsilon}\right),$$

$$\mathbf{v}_s(t,\mathbf{x}) = \frac{\mathbf{x}-\mathbf{x}_s}{4\pi\rho_0 c_0^2\varepsilon|\mathbf{x}-\mathbf{x}_s|^3}(\mathbf{x}-\mathbf{x}_s).\mathbf{f}'_{\mathbf{x}}\left(\frac{t-t_s-\frac{|\mathbf{x}-\mathbf{x}_s|}{c_0}}{\varepsilon}\right).$$

Note that the amplitude of the longitudinal velocity is one order of magnitude smaller than the other components. These expressions are derived from (2.24-2.25) and the Weyl representation of a spherical wave [24, Sec. 3.2.4], but they could also been derived directly from the fact that a point source emits a spherical wave that propagates at velocity c_0 in homogeneous medium. Let us next consider the evolution of the time-reversed field. For the sake of simplicity we address the case with a spatial mirror that has point support so that $\hat{G}_2(\mathbf{k})$ is a constant denoted by $\hat{g}_2$. In this case we find that

$$p_{TR}(t,\mathbf{x}) = -\frac{\rho_1 c_1\hat{g}_2}{(4\pi)^2\rho_0^3 c_0^3}\frac{1}{|\mathbf{x}_s|^3|\mathbf{x}|^2}(\mathbf{x}.\mathbf{x}_s)G_1\left(\frac{|\mathbf{x}|}{c_0}-t\right)\mathbf{x}_s.\mathbf{f}''_{\mathbf{x}}\left(\frac{\frac{|\mathbf{x}|-|\mathbf{x}_s|}{c_0}-t-t_s}{\varepsilon}\right),$$

$$u_{TR}(t,\mathbf{x}) = -\frac{\varepsilon^2\rho_1 c_1 \hat{g}_2}{(4\pi)^2\rho_0^2 c_0^2}\frac{1}{|\mathbf{x}_s|^2|\mathbf{x}|^2}G_1\left(\frac{|\mathbf{x}|}{c_0}-t\right)f_z\left(\frac{\frac{|\mathbf{x}|-|\mathbf{x}_s|}{c_0}-t-t_s}{\varepsilon}\right),$$

$$\mathbf{v}_{TR}(t,\mathbf{x}) = -\frac{\rho_1 c_1 \hat{g}_2}{(4\pi)^2\rho_0^2 c_0^4}\frac{1}{|\mathbf{x}_s|^3|\mathbf{x}|^3}\mathbf{x}(\mathbf{x}.\mathbf{x}_s)G_1\left(\frac{|\mathbf{x}|}{c_0}-t\right)\mathbf{x}_s.\mathbf{f}_{\mathbf{x}}''\left(\frac{\frac{|\mathbf{x}|-|\mathbf{x}_s|}{c_0}-t-t_s}{\varepsilon}\right).$$

Note that the longitudinal velocity field is actually vanishing (of order ε^2). Observe also that p_{TR} and $\mathbf{v}_{TR}$ are of order one only if the signal originating from the source has been recorded, meaning that $\frac{|\mathbf{x}_s|}{c_0}+t_s$ lies in the support of G_1, and if $(\frac{|\mathbf{x}|}{c_0}-t)-(\frac{|\mathbf{x}_s|}{c_0}+t_s)$ lies in the support of f corresponding to the propagation of a spherical wave from the mirror.

3.2. The random case. From now on we address the case of a random medium. We first consider the P_1 term of the expression (2.28) of the longitudinal velocity. We shall see in Appendix A.2 that the reflection coefficients at two frequencies and slowness vectors are correlated only if the frequencies and the moduli of the slowness vectors are close to each other at order ε. We accordingly perform the change of variables $\mu' = \mu_c + \varepsilon\lambda/2$ and $\mu = \mu_c - \varepsilon\lambda/2$. The representation of the P_1 term of the longitudinal velocity field becomes

$$u_{TR}^{(1)}(t,\mathbf{x}=r_0\mathbf{e}_{\theta_0},0) = -\frac{1}{(2\pi)^6\varepsilon}\int\int\frac{H_0(\mu_c\mathbf{e}_\theta,\mu_c\mathbf{e}_{\theta'})}{4\sqrt{I_0(\mu_c)}}\overline{\hat{G}_1}(-h)\hat{G}_2(\omega_c\mu_c(\mathbf{e}_\theta+\mathbf{e}_{\theta'}))$$
$$\times\overline{S_b}(\omega_c,\mu_c\mathbf{e}_{\theta'})e^{i\frac{\phi(\omega_c,\mu_c,\theta,\theta')}{\varepsilon}}e^{\frac{i}{2}\left(h(t-t_s)+(\lambda\omega_c+h\mu_c)[r_s\cos(\theta_s-\theta')-r_0\cos(\theta_0-\theta)]\right)}$$
$$(3.1)\times\overline{R}(\omega_c+\frac{\varepsilon h}{2},\mu_c+\frac{\varepsilon\lambda}{2},-L,0)R(\omega_c-\frac{\varepsilon h}{2},\mu_c-\frac{\varepsilon\lambda}{2},-L,0)\omega_c^4\mu_c^2 d\lambda dh d\omega_c d\mu_c d\theta d\theta'$$

where the rapid phase is

$$\phi(\omega_c,\mu_c,\theta,\theta') = \omega_c\left[-(t_s+t)+\mu_c(r_s\cos(\theta_s-\theta')+r_0\cos(\theta_0-\theta))\right]$$

and we have neglected lower order terms (with respect to ε) by assuming that H_0 and $\hat{G}_2$ are smooth functions. As $\varepsilon\to 0$ the asymptotic behavior of this integral is governed by its fast phase and by the product of the two reflection coefficients which contains the effect of randomness. We first apply the **stationary phase method** and we will deal with the random part of the integral in a second step. The variables of the rapid phase are ω_c, μ_c, θ, and θ'. We find that there exist stationary points only if $t+t_s=0$ and $r_0=r_s$. Then there exist two maps of stationary points corresponding to

$$I)\ \theta'=\theta_s \text{ and } \theta=\theta_0+\pi, \qquad II)\ \theta'=\theta_s+\pi \text{ and } \theta=\theta_0$$

We then consider an observation time t close to $-t_s$. Similarly we consider an observation point $\mathbf{x}$ whose modulus is close to r_s. This is realized by the following parameterization $t=-t_s+\varepsilon\mathcal{T}$, $\mathbf{x}=r_s\mathbf{e}_{\theta_0}+\varepsilon\mathcal{R}\mathbf{e}_\phi$. We deduce that the P_1 term of the longitudinal velocity field consists of the sum of two terms corresponding to the contributions of the two maps of stationary points and we write

$$u_{TR}^{(1)}(t,\mathbf{x},0) = u_{TR}^{(1,I)}(t,\mathbf{x},0)+u_{TR}^{(1,II)}(t,\mathbf{x},0)$$

with

$$u_{TR}^{(1,I)}(t,\mathbf{x},0) = -\frac{1}{2^7\pi^5 r_s}\int\int\frac{H_0(-\mu_c\mathbf{e}_{\theta_0},\mu_c\mathbf{e}_{\theta_s})}{\sqrt{I_0(\mu_c)}}\overline{\hat{G}_1}(-h)\hat{G}_2(\omega_c\mu_c(\mathbf{e}_{\theta_s}-\mathbf{e}_{\theta_0}))$$

$$\times\overline{S_b}(\omega_c,\mu_c\mathbf{e}_{\theta_s})e^{i(-\omega_c\mathcal{T}-ht_s+r_s(\lambda\omega_c+h\mu_c)-\omega_c\mu_c\mathcal{R}\cos(\theta_0-\phi))}$$
$$\times\overline{R}(\omega_c+\frac{\varepsilon h}{2},\mu_c+\frac{\varepsilon\lambda}{2},-L,0)R(\omega_c-\frac{\varepsilon h}{2},\mu_c-\frac{\varepsilon\lambda}{2}-L,0)\omega_c^3\mu_c d\lambda dh d\omega_c d\mu_c,$$

and

$$u_{TR}^{(1,II)}(t,\mathbf{x},0)=-\frac{1}{2^7\pi^5 r_s}\int\int\frac{H_0(\mu_c\mathbf{e}_{\theta_0},-\mu_c\mathbf{e}_{\theta_s})}{\sqrt{I_0(\mu_c)}}\overline{\hat{G}_1}(-h)\hat{G}_2(\omega_c\mu_c(\mathbf{e}_{\theta_0}-\mathbf{e}_{\theta_s}))$$
$$\times\overline{S_b}(\omega_c,-\mu_c\mathbf{e}_{\theta_s})e^{i(-\omega_c\mathcal{T}-ht_s-r_s(\lambda\omega_c+h\mu_c)+\omega_c\mu_c\mathcal{R}\cos(\theta_0-\phi))}$$
$$\times\overline{R}(\omega_c+\frac{\varepsilon h}{2},\mu_c+\frac{\varepsilon\lambda}{2}-L,0)R(\omega_c-\frac{\varepsilon h}{2},\mu_c-\frac{\varepsilon\lambda}{2}-L,0)\omega_c^3\mu_c d\lambda dh d\omega_c d\mu_c.$$

The effect of the randomness is contained in the product of the reflection coefficients. In the next section we exploit the asymptotic analysis of the autocorrelation function summarized in Appendix A.2 to deduce the refocusing properties of the pulse.

3.3. Refocusing of the pulse. The main result of this section is the refocusing of the pulse and its self-averaging property. The deterministic component of the time reversed wave given by the P_3 term is a spherical wave that is explicitly known and described in Section 3.1. Therefore it can be easily subtracted from the time reversed wave so that we deal only with the P_1, P_2, and P_4 terms. Using the last remark of Appendix A.2, one can deduce that the contributions of the P_2 and P_4 terms vanish in the limit $\varepsilon\to 0$, so we only need to study the P_1 term. Our stationary phase analysis presented in Section 3.2 shows that, for fixed observation time t and position $\mathbf{x}$, with $t+t_s\neq 0$ or $|\mathbf{x}|-r_s\neq 0$, there are no stationary points and $u_{TR}(t,\mathbf{x},0)$ goes to 0 as $\varepsilon\to 0$. On the other hand, if $t=-t_s$ and $|\mathbf{x}|=r_s$, then there are maps of stationary points so a refocused pulse with amplitude of order one will be observed in an ε-neighborhood of $(-t_s,r_s)$. These results are precisely stated in the following theorem which gives the refocusing property and the convergence of the refocused pulse to a deterministic shape concentrated at $-t_s$ in time and on a ring with radius r_s in space.

THEOREM 3.1. *a) For any $\mathcal{T}_0>0$, $\mathcal{R}_0>0$, $\delta>0$, and $(t_0,r_0)\neq(-t_s,r_s)$, we have*

$$\mathbb{P}\left(\sup_{|t-t_0|\leq\varepsilon\mathcal{T}_0,||\mathbf{x}|-r_0|\leq\varepsilon\mathcal{R}_0}|u_{TR}(t,\mathbf{x})|>\delta\right)\stackrel{\varepsilon\to 0}{\longrightarrow}0.$$

b) For any $\mathcal{T}_0>0$, $\mathcal{R}_0>0$, $\delta>0$, we have

$$\mathbb{P}\left(\sup_{|t+t_s|\leq\varepsilon\mathcal{T}_0,||\mathbf{x}|-r_s|\leq\varepsilon\mathcal{R}_0}\left|u_{TR}(t,\mathbf{x})-U_{TR}(\frac{t+t_s}{\varepsilon},\frac{|\mathbf{x}|-r_s}{\varepsilon})\right|>\delta\right)\stackrel{\varepsilon\to 0}{\longrightarrow}0$$

where U_{TR} is the deterministic pulse shape

$$U_{TR}(\mathcal{T},\mathcal{R})=\frac{1}{(2\pi)^3}\int\frac{1}{\sqrt{I_0(\mu)}}\left[\mathbf{K}_{\mathbf{x}}(\omega,\mu).\overline{\hat{\mathbf{f}}_{\mathbf{x}}}(\omega)+K_z(\omega,\mu)\overline{\hat{f}_z}(\omega)\right]e^{i\omega(\mu\mathcal{R}-\mathcal{T})}\omega^2 d\omega d\mu,$$

the kernels $\mathbf{K}_{\mathbf{x}}$ and K_z are given by

$$\mathbf{K}_{\mathbf{x}}(\omega,\mu)=K(\omega,\mu)\frac{\sqrt{I_0(\mu)}\mu}{2\rho_0}\mathbf{e}_{\theta_s}$$
$$K_z(\omega,\mu)=K(\omega,\mu)\frac{1}{2\sqrt{I_0(\mu)}}$$

with

$$K(\omega,\mu)=\hat{G}_2\left(\omega\mu(\mathbf{e}_{\theta_0}-\mathbf{e}_{\theta_s})\right)G_1(t_s+\frac{r_s}{c_0^2\mu})Q_1(\frac{\zeta_0(\mu)}{2\mu}r_s)\frac{\zeta_0(\mu)}{2}\frac{H_0(\mu\mathbf{e}_{\theta_0},-\mu\mathbf{e}_{\theta_s})}{2r_s}.$$

Q_1 is given by Eq. (A.3). An explicit expression for H_0 is

$$H_0(\mu\mathbf{e}_{\theta_0},-\mu\mathbf{e}_{\theta_s})=\zeta_0(\mu)c_0+\frac{c_0\mu^2}{\zeta_0(\mu)}\mathbf{e}_{\theta_0}.\mathbf{e}_{\theta_s}.$$

Similarly, the asymptotic deterministic shapes of the refocused transverse velocity and pressure fields consist of the sums of the deterministic components exhibited in Section 3.1 and of the new components:

$$P_{TR}(\mathcal{T},\mathcal{R})=\frac{1}{(2\pi)^3}\int\sqrt{I_0(\mu)}\left[K_{\mathbf{x}}(\omega,\mu).\overline{\hat{\mathbf{f}}_{\mathbf{x}}}(\omega)+K_z(\omega,\mu)\overline{\hat{f}_z}(\omega)\right]e^{i\omega(\mu\mathcal{R}-\mathcal{T})}\omega^2d\omega d\mu$$

$$\mathbf{V}_{TR}(\mathcal{T},\mathcal{R})=\frac{\mathbf{e}_{\theta_0}}{(2\pi)^3}\int\frac{\sqrt{I_0(\mu)}\mu}{\rho_0}\left[K_{\mathbf{x}}(\omega,\mu).\overline{\hat{\mathbf{f}}_{\mathbf{x}}}(\omega)+K_z(\omega,\mu)\overline{\hat{f}_z}(\omega)\right]e^{i\omega(\mu\mathcal{R}-\mathcal{T})}\omega^2d\omega d\mu$$

The proof of the theorem is a generalization of the arguments given in [9] and goes along the following main steps.
- We first consider the expected value of $u_{TR}^{(1)}$. Using a combination of stationary phase and the asymptotic behavior (A.4) of the autocorrelation function of the reflection coefficient we find that this expectation converges to the limiting value given in the theorem.
- We then consider the variance of $u_{TR}^{(1)}$. We write the second moment as a multiple integral involving the product of four reflection coefficients at four different frequencies as in (A.5). Using the decorrelation property of the reflection coefficient we deduce that the variance goes to zero.
Note that an integral over frequency (ensured by the time domain nature of time-reversal) is needed for the stabilization or the self-averaging of the refocused pulse. Applications of this result to the problem of the location of the source will be discussed in Section 5.

4. Interior point source. In this section we assume that the source is somewhere below the surface ($\mathbf{x}_s, z_s < 0$). The time-reversal strategy is the same as in the previous section, we shall obtain analogous results but the computations are more complicated and do not lead to fully explicit formulas such as the ones presented in Theorem 3.1. We start by considering the case of a homogeneous medium, as we shall study the problem of the source location and contrast the homogeneous and random configurations.

4.1. Homogeneous medium. The following expressions are straightforward generalizations of the ones presented in Section 3.1. The signal that can be recorded at the surface is a spherical wave. Using the notation $\mathbf{r}=(\mathbf{x},z)$ the pressure signal is

$$p_s(t,\mathbf{r})=\frac{1}{4\pi c_0\varepsilon|\mathbf{r}-\mathbf{r}_s|^2}(\mathbf{r}-\mathbf{r}_s).\begin{pmatrix}\mathbf{f}'_{\mathbf{x}}\\ f'_z\end{pmatrix}\left(\frac{t-t_s-\frac{|\mathbf{r}-\mathbf{r}_s|}{c_0}}{\varepsilon}\right)$$

while the three-dimensional velocity field is

$$\mathbf{u}_s(t,\mathbf{r})=\frac{\mathbf{r}-\mathbf{r}_s}{4\pi\rho_0c_0^2\varepsilon|\mathbf{r}-\mathbf{r}_s|^3}(\mathbf{r}-\mathbf{r}_s).\begin{pmatrix}\mathbf{f}'_{\mathbf{x}}\\ f'_z\end{pmatrix}\left(\frac{t-t_s-\frac{|\mathbf{r}-\mathbf{r}_s|}{c_0}}{\varepsilon}\right) \tag{4.1}$$

We consider again the time-reversed field in the case of a point mirror characterized by $\hat{G}_2(\mathbf{k}) \equiv \hat{g}_2$. The time reversed wave is then given by

$$p_{TR}(t,\mathbf{r}) = -\frac{\hat{g}_2}{(4\pi)^2\rho_0^2 c_0^2}\frac{1}{|\mathbf{r}_s|^3|\mathbf{r}|^2}(\mathbf{r}.\mathbf{r}_s)G_1\left(\frac{|\mathbf{r}|}{c_0}-t\right)\mathbf{r}_s.\begin{pmatrix}\mathbf{f}''_{\mathbf{x}}\\ f''_z\end{pmatrix}\left(\frac{\frac{|\mathbf{r}|-|\mathbf{r}_s|}{c_0}-t-t_s}{\varepsilon}\right)$$

(4.2) $$u_{TR}(t,\mathbf{r}) = -\frac{\hat{g}_2}{(4\pi)^2\rho_0 c_0^3}\frac{\mathbf{r}}{|\mathbf{r}_s|^3|\mathbf{r}|^3}(\mathbf{r}.\mathbf{r}_s)G_1\left(\frac{|\mathbf{r}|}{c_0}-t\right)\mathbf{r}_s.\begin{pmatrix}\mathbf{f}''_{\mathbf{x}}\\ f''_z\end{pmatrix}\left(\frac{\frac{|\mathbf{r}|-|\mathbf{r}_s|}{c_0}-t-t_s}{\varepsilon}\right)$$

This is a spherical wave emerging from the mirror. Its support at a given time t is an ε neighborhood of the sphere with center at $\mathbf{0}$ and radius $|\mathbf{r}_s| + c_0(t+t_s)$.

4.2. The stationary phase in the random case. We consider the P_1 term in the representation of the longitudinal velocity (2.28) with arbitrary z_s (depth of the source) and z (depth of the observation point). The other terms can be treated in the same way and we will collect and discuss all the contributions in Section 4.4. Once again, the generalized reflection coefficients at two different slowness vectors are correlated only if the moduli of the slowness vectors are close to each other at order ε. We accordingly perform the change of variables $\mu' = \mu_c + \varepsilon\lambda/2$ and $\mu = \mu_c - \varepsilon\lambda/2$, so that the representation of the P_1 term of the longitudinal velocity field becomes

$$\begin{aligned}u^{(1)}_{TR}(t,\mathbf{x}=r_0\mathbf{e}_{\theta_0},z) = -\frac{1}{(2\pi)^6\varepsilon}\int\int \frac{H_0(\mu_c\mathbf{e}_\theta,\mu_c\mathbf{e}_{\theta'})}{4\sqrt{I_0(\mu_c)}}\overline{\hat{G}_1}(-h)\hat{G}_2(\omega_c\mu_c(\mathbf{e}_\theta+\mathbf{e}_{\theta'}))\\ \times\overline{S_b}(\omega_c,\mu_c\mathbf{e}_{\theta'})e^{i\frac{\phi(\omega_c,\mu_c,\theta,\theta')}{\varepsilon}}e^{\frac{i}{2}\left(h(t-t_s)+(\lambda\omega_c+h\mu_c)[r_s\cos(\theta_s-\theta')-r_0\cos(\theta_0-\theta)]\right)}\\ \times e^{-\frac{i}{2}\left([h\zeta_0(\mu_c)+\omega_c\zeta_0'(\mu_c)\lambda](z+z_s)\right)}\\ \times\overline{R_g}(\omega_c+\frac{\varepsilon h}{2},\mu_c+\frac{\varepsilon\lambda}{2},z_s)R_g(\omega_c-\frac{\varepsilon h}{2},\mu_c-\frac{\varepsilon\lambda}{2},z)\omega_c^4\mu_c^2 d\lambda dh d\omega_c d\mu_c d\theta d\theta'\end{aligned} \tag{4.3}$$

where $\zeta_0'(\mu_c) = -\mu_c/\zeta_0(\mu_c)$ and the rapid phase is

$$\phi(\omega_c,\mu_c,\theta,\theta') = \omega_c\left[-(t_s+t)+\mu_c(r_s\cos(\theta_s-\theta')+r_0\cos(\theta_0-\theta))+\zeta_0(\mu_c)(z-z_s)\right].$$

As in Section 3.2 we first apply the stationary phase method and we will deal with the random part of the integral (the product of the two generalized reflection coefficients) in a second step. The variables of the rapid phase are ω_c, μ_c, θ, and θ', and the partial derivatives of ϕ are

$$\begin{aligned}\frac{\partial\phi}{\partial\omega_c} &= -(t_s+t)+\mu_c(r_s\cos(\theta_s-\theta')+r_0\cos(\theta_0-\theta))+\zeta_0(\mu_c)(z-z_s)\\ \frac{\partial\phi}{\partial\mu_c} &= \omega_c(r_s\cos(\theta_s-\theta')+r_0\cos(\theta_0-\theta))+\omega_c\zeta_0'(\mu_c)(z-z_s)\\ \frac{\partial\phi}{\partial\theta} &= \omega_c\mu_c r_0\sin(\theta_0-\theta)\\ \frac{\partial\phi}{\partial\theta'} &= \omega_c\mu_c r_s\sin(\theta_s-\theta').\end{aligned}$$

Assuming first that $\mathbf{r}_s \neq 0$, that is the case where the mirror is not directly above the source, there are several possible configurations. Using the notation

$$\mu_c^\star = c_0^{-1}\sqrt{1-(z-z_s)^2/c_0^2(t+t_s)^2}$$

when $(z-z_s)^2 \le c_0^2(t+t_s)^2$, we get:

1. If $c_0^2(t+t_s)^2 = (r_s - r_0)^2 + (z - z_s)^2$ with $z > z_s$ and $t + t_s > 0$, then there exists one map of stationary points corresponding to

$$\begin{aligned} &\text{if } r_0 > r_s \text{ then } \theta' = \theta_s + \pi,\ \theta = \theta_0, \text{ and } \mu_c = \mu_c^\star \\ &\text{if } r_0 < r_s \text{ then } \theta' = \theta_s,\ \theta = \theta_0 + \pi, \text{ and } \mu_c = \mu_c^\star \end{aligned}$$

   with no restriction on ω_c.
2. If $c_0^2(t+t_s)^2 = (r_s - r_0)^2 + (z - z_s)^2$ with $z < z_s$ and $t + t_s < 0$, then there exists one map of stationary points corresponding to

$$\begin{aligned} &\text{if } r_0 > r_s \text{ then } \theta' = \theta_s,\ \theta = \theta_0 + \pi, \text{ and } \mu_c = \mu_c^\star \\ &\text{if } r_0 < r_s \text{ then } \theta' = \theta_s + \pi,\ \theta = \theta_0, \text{ and } \mu_c = \mu_c^\star \end{aligned}$$

   with no restriction on ω_c.
3. If $c_0^2(t+t_s)^2 = (r_s + r_0)^2 + (z - z_s)^2$ with $z > z_s$ and $t + t_s > 0$, then there exists one map of stationary points corresponding to

$$\theta' = \theta_s,\ \theta = \theta_0, \text{ and } \mu_c = \mu_c^\star$$

   with no restriction on ω_c.
4. If $c_0^2(t+t_s)^2 = (r_s + r_0)^2 + (z - z_s)^2$ with $z < z_s$ and $t + t_s < 0$, then there exists one map of stationary points corresponding to

$$\theta' = \theta_s + \pi, \theta = \theta_0 + \pi, \text{ and } \mu_c = \mu_c^\star$$

   with no restriction on ω_c.
5. If $t + t_s = 0$, $r_0 = r_s$, and $z = z_s$, then there exist two maps of stationary points corresponding to

$$\begin{aligned} &I)\ \theta' = \theta_s \text{ and } \theta = \theta_0 + \pi \\ &II)\ \theta' = \theta_s + \pi \text{ and } \theta = \theta_0 \end{aligned}$$

   with no restriction on ω_c and μ_c.

Note that other maps with $\omega_c = 0$ or $\mu_c = 0$ do not lead to significant contributions because of the presence of the factor $\omega_c^4 \mu_c^2$ in the integral representation of $u_{TR}^{(1)}$. In configurations 1-4 the stationary maps are of dimension 3 and the stationary phase method gives an effective value for the integral which is of order $\varepsilon^{3/2}$ and consequently contributes to a term of order $\varepsilon^{1/2}$ to $u_{TR}^{(1)}$. In configuration 5, because of the additional degeneracy in μ_c, the stationary maps are two-dimensional and the stationary phase method gives an effective value for the integral which is of order ε and consequently only configuration 5 contributes to a term of order one to $u_{TR}^{(1)}$. In other words, this component of the time reversed wave is only observed at the right time $-t_s$, at the right depth z_s, and on the ring with radius r_s. We accordingly consider an observation time t close to $-t_s$, and an observation point $(\mathbf{x}, z)$ which is such that z is close to z_s and the modulus of $\mathbf{x}$ is close to r_s. We do so by writing $t = -t_s + \varepsilon\mathcal{T}$, $\mathbf{x} = r_s \mathbf{e}_{\theta_0} + \varepsilon\mathcal{R}\mathbf{e}_\phi$, and $z = z_s + \varepsilon\mathcal{Z}$. We get that, to leading order in ε, the P_1 term of the longitudinal velocity field consists of the sum of two terms corresponding to the contributions of the two maps of stationary points (5-I and 5-II)

$$u_{TR}^{(1)}(t, \mathbf{x}, z) = u_{TR}^{(1,I)}(t, \mathbf{x}, z) + u_{TR}^{(1,II)}(t, \mathbf{x}, z)$$

with

$$u_{TR}^{(1,I)}(t,\mathbf{x},z) = -\frac{1}{2^7\pi^5 r_s}\int\int \frac{H_0(-\mu_c\mathbf{e}_{\theta_0},\mu_c\mathbf{e}_{\theta_s})}{\sqrt{I_0(\mu_c)}}\overline{\hat{G}_1}(-h)\hat{G}_2(\omega_c\mu_c(\mathbf{e}_{\theta_s}-\mathbf{e}_{\theta_0}))$$
$$\times\overline{S_b}(\omega_c,\mu_c\mathbf{e}_{\theta_s})e^{i(-\omega_c\mathcal{T}-\omega_c\mu_c\mathcal{R}\cos(\theta_0-\phi)+\omega_c\zeta_0(\mu_c)\mathcal{Z})}$$
$$\times e^{i\left(-ht_s+r_s(\lambda\omega_c+h\mu_c)-[h\zeta_0(\mu_c)+\omega_c\zeta_0'(\mu_c)\lambda]z_s\right)}$$
$$\times\overline{R_g}(\omega_c+\frac{\varepsilon h}{2},\mu_c+\frac{\varepsilon\lambda}{2},z_s)R_g(\omega_c-\frac{\varepsilon h}{2},\mu_c-\frac{\varepsilon\lambda}{2},z_s+\varepsilon\mathcal{Z})\omega_c^3\mu_c d\lambda dh d\omega_c d\mu_c$$

$$u_{TR}^{(1,II)}(t,\mathbf{x},z) = -\frac{1}{2^7\pi^5 r_s}\int\int \frac{H_0(\mu_c\mathbf{e}_{\theta_0},-\mu_c\mathbf{e}_{\theta_s})}{\sqrt{I_0(\mu_c)}}\overline{\hat{G}_1}(-h)\hat{G}_2(\omega_c\mu_c(\mathbf{e}_{\theta_0}-\mathbf{e}_{\theta_s}))$$
$$\times\overline{S_b}(\omega_c,-\mu_c\mathbf{e}_{\theta_s})e^{i(-\omega_c\mathcal{T}+\omega_c\mu_c\mathcal{R}\cos(\theta_0-\phi)+\omega_c\zeta_0(\mu_c)\mathcal{Z})}$$
$$\times e^{i\left(-ht_s-r_s(\lambda\omega_c+h\mu_c)-[h\zeta_0(\mu_c)+\omega_c\zeta_0'(\mu_c)\lambda]z_s\right)}$$
$$\times\overline{R_g}(\omega_c+\frac{\varepsilon h}{2},\mu_c+\frac{\varepsilon\lambda}{2},z_s)R_g(\omega_c-\frac{\varepsilon h}{2},\mu_c-\frac{\varepsilon\lambda}{2},z_s+\varepsilon\mathcal{Z})\omega_c^3\mu_c d\lambda dh d\omega_c d\mu_c$$

This integral representation of the signal shows that the autocorrelation function of the generalized reflection coefficient defined by (2.20) plays a key role. Before going into the details of the asymptotics of $u_{TR}^{(1)}$ in the case $r_s \neq 0$, we observe that the case where the mirror is exactly above the source, that is $r_s = 0$, is particular.

Mirror above the source $r_s = 0$. In this case the analysis of the stationary phase exhibits the following configurations.

1. If $r_0 \neq 0$, $r_0^2 + (z-z_s)^2 = c_0^2(t+t_s)^2$, $z - z_s > 0$, and $t + t_s > 0$, then there exists one map of stationary points corresponding to
$$\theta = \theta_0 \text{ and } \mu_c = \frac{r_0}{c_0^2(t+t_s)}$$
with no restriction on ω_c and θ'.
2. If $r_0 \neq 0$, $r_0^2 + (z-z_s)^2 = c_0^2(t+t_s)^2$, $z - z_s < 0$, and $t + t_s < 0$, then there exists one map of stationary points corresponding to
$$\theta = \theta_0 + \pi \text{ and } \mu_c = \frac{r_0}{c_0^2|t+t_s|}$$
with no restriction on ω_c and θ'.
3. If $r_0 = 0$, $z = z_s$, and $t + t_s = 0$, then the rapid phase is fully degenerated.

Configuration 3 corresponds to the critical time where the time reversed wave refocuses. It contributes a term which is of order ε^{-1} to $u_{TR}^{(1)}$ at the exact location of the original source. This result is not surprising. Indeed, in contrast with the general case $r_s \neq 0$, the wave refocuses on a single point instead of refocusing on a ring, which makes the amplitude blow up. We could alternatively have rescaled the initial source by a factor ε and the contribution in that case is of order one. From the point of view of applications, as we will see in Section 5, the generic case is $r_s \neq 0$ which justifies the scaling of order one in the amplitude of the initial source given in (1.5).

4.3. Asymptotics of the first moment of $u_{TR}^{(1)}$. The computation of the expectation of the P_1 term of the integral representation of $u_{TR}^{(1)}$ is reduced to the computation of the quantity

$$U_g^\varepsilon = \mathbb{E}\left[\overline{R_g}(\omega_c+\frac{\varepsilon h}{2},\mu_c+\frac{\varepsilon\lambda}{2},z_s)R_g(\omega_c-\frac{\varepsilon h}{2},\mu_c-\frac{\varepsilon\lambda}{2},z_s+\varepsilon\mathcal{Z})\right]$$

Using the representation (2.22) of the generalized coefficient R_g in terms of the usual reflection and transmission coefficients, we obtain that

$$U_g^\varepsilon = \sum_{n,m=0}^{\infty} \mathbb{E}\left[\overline{R}^{n+1}\ R^{m+1}\ \widetilde{R}^n \widetilde{T}\ \overline{\widetilde{R}}^m \overline{\widetilde{T}}\right]$$

where $\overline{R}^{n+1}$ is evaluated at $(\omega_c + \varepsilon h/2, \mu_c + \varepsilon\lambda/2, -L, z_s)$, R^{m+1} is evaluated at $(\omega_c - \varepsilon h/2, \mu_c - \varepsilon\lambda/2, -L, z_s + \varepsilon\mathcal{Z})$, $\widetilde{R}^n \widetilde{T}$ is evaluated at $(\omega_c + \varepsilon h/2, \mu_c + \varepsilon\lambda/2, z_s, 0)$, and $\overline{\widetilde{R}}^n \overline{\widetilde{T}}$ is evaluated at $(\omega_c - \varepsilon h/2, \mu_c - \varepsilon\lambda/2, z_s + \varepsilon\mathcal{Z}, 0)$. As $\varepsilon \to 0$ the propagators between $-L$ and z_s and between z_s and 0 become independent. By continuity with respect to z of the limits of the moments of the reflection and transmission coefficients, the $\varepsilon\mathcal{Z}$ does not play any role in the limit of U_g^ε. Accordingly we shall obtain the limit of U_g^ε as $\varepsilon \to 0$ by looking at the limits of $\mathbb{E}[\overline{R}^{n+1} R^{m+1}]$ and $\mathbb{E}[\widetilde{R}^n \widetilde{T} \overline{\widetilde{R}}^m \overline{\widetilde{T}}]$. By using the shift properties of the reflection coefficients described in Appendix A.4 and the expressions of the limit values for moments of reflection and transmission coefficients, we obtain that

$$\mathbb{E}\left[R^{n+1}\overline{R}^{m+1}\right] \overset{\varepsilon\to 0}{\longrightarrow} \begin{cases} 0 & \text{if } m \neq n \\ e^{2i(n+1)[h\zeta_0(\mu_c)+\lambda\omega_c\zeta_0'(\mu_c)]z_s} & \\ \times \int W_{n+1}(\tau, \omega_c, \mu_c, -L, z_s) e^{i\tau(c_0^2\omega_c\mu_c\lambda - h(1-c_0^2\mu_c^2)} d\tau & \text{if } m = n \end{cases}$$

$$\mathbb{E}\left[\widetilde{R}^n \widetilde{T}\ \overline{\widetilde{R}}^m \overline{\widetilde{T}}\right] \overset{\varepsilon\to 0}{\longrightarrow} \begin{cases} 0 & \text{if } m \neq n \\ e^{-2in[h\zeta_0(\mu_c)+\lambda\omega_c\zeta_0'(\mu_c)]z_s} & \\ \times \int \widetilde{W}_n(\tau, \omega_c, \mu_c, z_s, 0) e^{i\tau(c_0^2\omega_c\mu_c\lambda - h(1-c_0^2\mu_c^2)} d\tau & \text{if } m = n \end{cases}$$

where W_n and $\widetilde{W}_n$ are described in Appendices A.2 and A.3 respectively. We can then deduce that

$$U_g^\varepsilon \overset{\varepsilon\to 0}{\longrightarrow} \sum_{n=0}^{\infty} e^{2i[h\zeta_0(\mu_c)+\lambda\omega_c\zeta_0'(\mu_c)]z_s} \int W_{n+1}(\tau, \omega_c, \mu_c) e^{i\tau H} d\tau \int \widetilde{W}_n(\tau, \omega_c, \mu_c) e^{i\tau H} d\tau$$

where $H = c_0^2\omega_c\mu_c\lambda - h(1 - c_0^2\mu_c^2)$. Substituting the limit of U_g^ε in the integral representations of $u_{TR}^{(1,I)}$ and $u_{TR}^{(1,II)}$ we find that

$$\mathbb{E}[u_{TR}^{(1,I)}(t, \mathbf{x}, z)] \overset{\varepsilon\to 0}{\longrightarrow} \frac{-1}{2^5\pi^3 r_s c_0^2} \int \frac{H_0(-\mu_c \mathbf{e}_{\theta_0}, \mu_c \mathbf{e}_{\theta_s})}{\sqrt{I_0(\mu_c)}} \hat{G}_2(\omega_c\mu_c(\mathbf{e}_{\theta_s} - \mathbf{e}_{\theta_0})) \overline{S_b}(\omega_c, \mu_c \mathbf{e}_{\theta_s})$$
$$\times e^{i\omega_c[-\mathcal{T} - \mu_c\mathcal{R}\cos(\theta_0-\phi) + \zeta_0(\mu_c)\mathcal{Z}]} G_1\left(t_s - \frac{r_s}{c_0^2\mu_c}\right) W_{g,1}\left(\frac{-r_s + \frac{\mu_c}{\zeta_0(\mu_c)} z_s}{\mu_c c_0^2}\right) \omega_c^2 d\mu_c d\omega_c$$

$$\mathbb{E}[u_{TR}^{(1,II)}(t, \mathbf{x}, z)] \overset{\varepsilon\to 0}{\longrightarrow} \frac{-1}{2^5\pi^3 r_s c_0^2} \int \frac{H_0(\mu_c \mathbf{e}_{\theta_0}, -\mu_c \mathbf{e}_{\theta_s})}{\sqrt{I_0(\mu_c)}} \hat{G}_2(\omega_c\mu_c(\mathbf{e}_{\theta_0} - \mathbf{e}_{\theta_s})) \overline{S_b}(\omega_c, -\mu_c \mathbf{e}_{\theta_s})$$
$$\times e^{i\omega_c[-\mathcal{T} + \mu_c\mathcal{R}\cos(\theta_0-\phi) + \zeta_0(\mu_c)\mathcal{Z}]} G_1\left(t_s + \frac{r_s}{c_0^2\mu_c}\right) W_{g,1}\left(\frac{r_s + \frac{\mu_c}{\zeta_0(\mu_c)} z_s}{\mu_c c_0^2}\right) \omega_c^2 d\mu_c d\omega_c$$

where

$$W_{g,1}(\tau, \omega_c, \mu_c) = \sum_{n=0}^{\infty} \left[W_{n+1}(\cdot, \omega_c, \mu_c, -L, z_s) * \widetilde{W}_n(\cdot, \omega_c, \mu_c, z_s, 0)\right](\tau)$$

and $t = -t_s + \varepsilon\mathcal{T}$, $\mathbf{x} = r_s\mathbf{e}_{\theta_0} + \mathcal{R}\mathbf{e}_\phi$, and $z = z_s + \varepsilon\mathcal{Z}$. The probabilistic representations for W_n and $\widetilde{W}_n$ show that they vanish for $\tau < 0$, so that $W_{g,1}$ also vanishes for $\tau < 0$. As a consequence the limit of $\mathbb{E}[u_{TR}^{(1,I)}(t,\mathbf{x},z)]$ is zero, and only the second map contributes to the expected value of $u_{TR}^{(1)}$.

4.4. Other components to the first moment of u_{TR}. We have just addressed the P_1 term of the integral representation (2.28) of u_{TR}. We now consider the three other terms P_2, P_3, and P_4. The terms $u_{TR}^{(2)}$ and $u_{TR}^{(4)}$ associated with P_2 and P_4 have no stationary point because z and z_s appear with the same signs in their fast phases. Consequently these two terms do not contribute to the limit value of u_{TR} as $\varepsilon \to 0$. We now address the term $u_{TR}^{(3)}$ associated with P_3 given by Eq. (2.28). In this case, the generalized transmission coefficients at two different slowness vectors are always correlated. Consequently the domain of integration contributing to the value of the integral (2.28) is not restricted to an ε-neighborhood of the diagonal $\mu' \simeq \mu$. We thus split the domain of integration into two parts. The first part corresponds to a subdomain which is an ε-neighborhood of the diagonal. It can be treated as in the previous section where we dealt with the P_1 term. The second part contains the non-diagonal contribution to the integral which captures the coherent propagating front as described below.

4.4.1. Diagonal contribution. The integral representation of the diagonal contribution $u_{TR}^{(3,diag)}$ is similar to Eq. (4.3), but involves the product of two generalized transmission coefficients and appropriate phases. The random component can be expanded in terms of the standard transmission and reflection as

$$\overline{T_g}T_g = \sum_{n,m=0}^{\infty} \overline{R}^n \, R^m \, \widetilde{R}^n \widetilde{T} \, \overline{\widetilde{R}}^m \overline{\widetilde{T}}$$

Following the same strategy as in the previous sections and using the asymptotic analysis for the expectation of the moments of transmission-reflection coefficients presented in Appendix A.3, we get that the only configuration leading to an expected value of order one for $u_{TR}^{(3,diag)}$ is obtained when the observation coordinates t, z, and $|\mathbf{x}|$ are in an ε-neighborhood of $-t_s$ and r_s, and z_s, respectively. More precisely, taking $t = -t_s + \varepsilon\mathcal{T}$, $\mathbf{x} = r_s\mathbf{e}_{\theta_0} + \varepsilon\mathcal{R}\mathbf{e}_\phi$, and $z = z_s + \varepsilon\mathcal{Z}$, we get that

$$\mathbb{E}[u_{TR}^{(3,diag)}(t,\mathbf{x},z)] \overset{\varepsilon\to 0}{\longrightarrow} \frac{-1}{2^5\pi^3 r_s c_0^2} \int \frac{H_0(\mu_c\mathbf{e}_{\theta_0}, -\mu_c\mathbf{e}_{\theta_s})}{\sqrt{I_0(\mu_c)}} \hat{G}_2(\omega_c\mu_c(\mathbf{e}_{\theta_0} - \mathbf{e}_{\theta_s}))\overline{S_a}(\omega_c, -\mu_c\mathbf{e}_{\theta_s})$$
$$\times e^{i\omega_c[-\mathcal{T} - \mu_c\mathcal{R}\cos(\theta_0-\phi) - \zeta_0(\mu_c)\mathcal{Z}]} G_1\left(t_s + \frac{r_s}{c_0^2\mu_c}\right) W_{g,3}\left(\frac{r_s + \frac{\mu_c}{\zeta_0(\mu_c)}z_s}{\mu_c c_0^2}\right) \omega_c^2 d\mu_c d\omega_c$$

where

$$W_{g,3}(\tau,\omega_c,\mu_c) = \sum_{n=0}^{\infty} \Big[W_n(\cdot,\omega_c,\mu_c,-L,z-s) * \widetilde{W}_n(\cdot,\omega_c,\mu_c,z-s,0)\Big](\tau)$$

4.4.2. Off-diagonal contribution. The off-diagonal contribution $u_{TR}^{(3,off)}$ corresponds to the time reversal of the coherent front. It has been analyzed in detail in [13] in the case of time-reversal in transmission, so by a simple generalization using

the moment analysis presented in Appendix A.1, one can deduce that the coherent time-reversed front wave propagates like a spherical wave around

$$z^2 + |\mathbf{x}|^2 = c_0^2(t - t_c)^2, \quad t_c = -t_s - \frac{\sqrt{z_s^2 + r_s^2}}{c_0}$$

More precisely, if the mirror is pointwise so that $\hat{G}_2 = \hat{g}_2$, then $u_{TR}^{(3,off)}$ converges in distribution as $\varepsilon \to 0$ to

$$u_{TR}^{coh}(t, \mathbf{x}, z) = G_1(-t_c)\, u_{TR,\mathbf{x},z}^{hom} * K_{ODA,\mathbf{x},z}\left(\frac{\frac{|\mathbf{r}|-|\mathbf{r}_s|}{c_0} - t - t_s}{\varepsilon}\right)$$

where u_{TR}^{hom} is the front shape in homogeneous medium computed in Section 4.1 and given by

$$u_{TR,\mathbf{x},z}^{hom}(t) = -\frac{\hat{g}_2}{(4\pi)^2\rho_0 c_0^3} \frac{(\mathbf{x}.\mathbf{x}_s + z z_s)z}{\sqrt{r_s^2 + z_s^2}^3 \sqrt{|\mathbf{x}|^2 + z^2}^3} [\mathbf{x}_s.\mathbf{f}_{\mathbf{x}}''(t) + z_s f_z''(t)] \tag{4.4}$$

and K_{ODA} is the O'Doherty-Anstey (ODA) kernel whose Fourier transform is

$$\hat{K}_{ODA,\mathbf{x},z}(\omega) = \exp\left(i[\sqrt{\gamma(\omega,\mu)}B_z - \sqrt{\gamma(\omega,\mu')}B_{z_s}] + \frac{\gamma(\omega,\mu)z + \gamma(\omega,\mu')z_s}{2}\right) \tag{4.5}$$

with $\mu = \frac{1}{c_0}\frac{|\mathbf{x}|}{\sqrt{|\mathbf{x}|^2+z^2}}$, $\mu' = \frac{1}{c_0}\frac{r_s}{\sqrt{r_s^2+z_s^2}}$, B is a standard one-dimensional Brownian motion, and γ is given by (A.1). The shape of the front is deterministic and results from a first spreading due to the propagation from the source to the mirror cumulated with a second spreading due to the propagation from the mirror to the observation point. The effect of randomness also imposes a random shift of this deterministic shape which cancels out only if the observation is taken on the ring $z = z_s$ and $|\mathbf{x}| = r_s$.

4.5. Summary. We sum up the previous results in the next theorem. We assume a point mirror so that $\hat{G}_2(\mathbf{k}) = \hat{g}_2$. We also assume the generic case where the mirror is not exactly above the source, that is to say $r_s \neq 0$. We consider the time reversed wave and observe it in an ε-neighborhood of an arbitrary observation point (t_0, r_0, z_0). Three types of configurations can be distinguished. The first case (a) corresponds to an observation point outside of the support of the spherical front wave. The second case (b) corresponds to an observation point on the support of the spherical front wave but outside the refocusing ring. The third case (c) corresponds to an observation point on the refocusing ring. In the following theorem t_c is

$$t_c = -t_s - \frac{\sqrt{r_s^2 + z_s^2}}{c_0}$$

THEOREM 4.1. *a) If $c_0^2(t_0 - t_c)^2 \neq r_0^2 + z_0^2$, then, for any $\mathcal{T}_0 > 0$, $\mathcal{R}_0 > 0$, $\mathcal{Z}_0 > 0$, and $\delta > 0$, we have*

$$\mathbb{P}\left(\sup_{|\mathcal{T}|\leq\mathcal{T}_0, |\mathcal{R}|\leq\mathcal{R}_0, \theta_0\in[0,2\pi), |\mathcal{Z}|\leq\mathcal{Z}_0} |u_{TR}(t_0 + \varepsilon\mathcal{T}, (r_0 + \varepsilon\mathcal{R})\mathbf{e}_{\theta_0}, z_0 + \varepsilon\mathcal{Z})| > \delta\right) \overset{\varepsilon\to 0}{\longrightarrow} 0.$$

b) If $c_0^2(t_0-t_c)^2 = r_0^2+z_0^2$ *and* $t_0 \neq -t_s$, *then for any* $\mathcal{T}_0>0$, $\mathcal{R}_0>0$, *and* $\mathcal{Z}_0>0$, *we have the following convergence in distribution*

$$\begin{aligned}&(u_{TR}(t_0+\varepsilon\mathcal{T},(r_0+\varepsilon\mathcal{R})\mathbf{e}_{\theta_0},z_0+\varepsilon\mathcal{Z}))_{|\mathcal{T}|\leq\mathcal{T}_0,|\mathcal{R}|\leq\mathcal{R}_0,\theta_0\in[0,2\pi),|\mathcal{Z}|\leq\mathcal{Z}_0}\\ &\quad\stackrel{\varepsilon\to 0}{\longrightarrow} G_1(-t_c)\left[u^{hom}_{TR,r_0\mathbf{e}_{\theta_0},z_0}*K_{ODA,r_0\mathbf{e}_{\theta_0},z_0}\right]\left(\frac{r_0\mathcal{R}+z_0\mathcal{Z}}{c_0\sqrt{r_0^2+z_0^2}}-\mathcal{T}\right)\end{aligned}$$

where u^{hom}_{TR} *is the front shape in homogeneous medium given by (4.4) and* K_{ODA} *is the random kernel given by (4.5).*

c) If $c_0^2(t_0-t_c)^2 = r_0^2+z_0^2$, $t_0=-t_s$, *and* $z_0=z_s$ *(so* $r_0=r_s$*), then for any* $\mathcal{T}_0>0$, $\mathcal{R}_0>0$, $\mathcal{Z}_0$, *and* $\delta>0$, *we have*

$$\begin{aligned}\mathbb{P}\Bigg(\sup_{|\mathcal{T}|\leq\mathcal{T}_0,|\mathcal{R}|\leq\mathcal{R}_0,\theta_0\in[0,2\pi),|\mathcal{Z}|\leq\mathcal{Z}_0}&|u_{TR}(t_0+\varepsilon\mathcal{T},(r_0+\varepsilon\mathcal{R})\mathbf{e}_{\theta_0},z_0+\varepsilon\mathcal{Z})\\ &-U_{TR}(\mathcal{T},\mathcal{R},\mathcal{Z})|>\delta\Bigg)\stackrel{\varepsilon\to 0}{\longrightarrow}0\end{aligned}$$

where U_{TR} *is the deterministic pulse shape*

$$\begin{aligned}U_{TR}(\mathcal{T},\mathcal{R},\mathcal{Z}) &= u^{hom}_{TR,r_s\mathbf{e}_{\theta_0},z_s}*K_0\left(\frac{r_s\mathcal{R}+z_s\mathcal{Z}}{c_0\sqrt{r_s^2+z_s^2}}-\mathcal{T}\right)\\ &+\frac{1}{(2\pi)^3}\int\frac{1}{\sqrt{I_0(\mu)}}\left[\mathbf{K}^+_{\mathbf{x}}(\omega,\mu).\overline{\hat{\mathbf{f}}_{\mathbf{x}}}(\omega)+K^+_z(\omega,\mu)\overline{\hat{f}_z}(\omega)\right]e^{i\omega(\mu\mathcal{R}-\mathcal{T}+\zeta_0(\mu)\mathcal{Z})}\omega^2 d\omega d\mu\\ &+\frac{1}{(2\pi)^3}\int\frac{1}{\sqrt{I_0(\mu)}}\left[\mathbf{K}^-_{\mathbf{x}}(\omega,\mu).\overline{\hat{\mathbf{f}}_{\mathbf{x}}}(\omega)+K^-_z(\omega,\mu)\overline{\hat{f}_z}(\omega)\right]e^{i\omega(\mu\mathcal{R}-\mathcal{T}-\zeta_0(\mu)\mathcal{Z})}\omega^2 d\omega d\mu,\end{aligned}$$

u^{hom}_{TR} *is given by Eq. (4.4),*

$$\hat{K}_0(\omega)=G_1(-t_c)\exp\left(\frac{\gamma_0\omega^2(r_s^2+z_s^2)}{2c_0^2z_s}\right)$$

the kernels $\mathbf{K}^\pm_{\mathbf{x}}$ *and* $K^\pm_z$ *are given by*

$$\begin{aligned}\mathbf{K}^\pm_{\mathbf{x}}(\omega,\mu)&=K^\pm(\omega,\mu)\frac{\sqrt{I_0(\mu)}\mu}{2\rho_0}\mathbf{e}_{\theta_s},\\ K^\pm_z(\omega,\mu)&=K^\pm(\omega,\mu)\frac{1}{2\sqrt{I_0(\mu)}},\end{aligned}$$

with

$$\begin{aligned}K^+(\omega,\mu)&=G_1(t_s+\frac{r_s}{c_0^2\mu})W_{g,1}(\frac{r_s+\frac{\mu}{\zeta_0(\mu)}z_s}{\mu c_0^2})\frac{H_0(\mu\mathbf{e}_{\theta_0},-\mu\mathbf{e}_{\theta_s})}{2c_0^2r_s},\\ K^-(\omega,\mu)&=G_1(t_s+\frac{r_s}{c_0^2\mu})W_{g,3}(\frac{r_s+\frac{\mu}{\zeta_0(\mu)}z_s}{\mu c_0^2})\frac{H_0(\mu\mathbf{e}_{\theta_0},-\mu\mathbf{e}_{\theta_s})}{2c_0^2r_s}.\end{aligned}$$

An explicit expression for H_0 is

$$H_0(\mu\mathbf{e}_{\theta_0},-\mu\mathbf{e}_{\theta_s})=\zeta_0(\mu)c_0+\frac{c_0\mu^2}{\zeta_0(\mu)}\mathbf{e}_{\theta_0}.\mathbf{e}_{\theta_s}.$$

The picture is qualitatively the same for the time-reversed transverse velocity and pressure fields. The precise expressions for the refocused fields on the ring are the following ones:

$$P_{TR}(\mathcal{T},\mathcal{R},\mathcal{Z}) = p^{hom}_{TR,r_s\mathbf{e}_{\theta_0},z_s} * K_0\left(\frac{r_s\mathcal{R}+z_s\mathcal{Z}}{c_0\sqrt{r_s^2+z_s^2}}-\mathcal{T}\right)$$
$$+\frac{1}{(2\pi)^3}\int \sqrt{I_0(\mu)}\left[\mathbf{K}^+_{\mathbf{x}}(\omega,\mu).\overline{\hat{\mathbf{f}}_{\mathbf{x}}}(\omega)+K^+_z(\omega,\mu)\overline{\hat{f}_z}(\omega)\right]e^{i\omega(\mu\mathcal{R}-\mathcal{T}+\zeta_0(\mu)\mathcal{Z})}\omega^2 d\omega d\mu$$
$$+\frac{1}{(2\pi)^3}\int \sqrt{I_0(\mu)}\left[\mathbf{K}^-_{\mathbf{x}}(\omega,\mu).\overline{\hat{\mathbf{f}}_{\mathbf{x}}}(\omega)+K^-_z(\omega,\mu)\overline{\hat{f}_z}(\omega)\right]e^{i\omega(\mu\mathcal{R}-\mathcal{T}-\zeta_0(\mu)\mathcal{Z})}\omega^2 d\omega d\mu$$

$$\mathbf{V}_{TR}(\mathcal{T},\mathcal{R},\mathcal{Z}) = \mathbf{v}^{hom}_{TR,r_s\mathbf{e}_{\theta_0},z_s} * K_0\left(\frac{r_s\mathcal{R}+z_s\mathcal{Z}}{c_0\sqrt{r_s^2+z_s^2}}-\mathcal{T}\right)$$
$$+\frac{\mathbf{e}_{\theta_0}}{(2\pi)^3}\int \frac{\sqrt{I_0(\mu)}\mu}{\rho_0}\left[\mathbf{K}^+_{\mathbf{x}}(\omega,\mu).\overline{\hat{\mathbf{f}}_{\mathbf{x}}}(\omega)+K^+_z(\omega,\mu)\overline{\hat{f}_z}(\omega)\right]e^{i\omega(\mu\mathcal{R}-\mathcal{T}+\zeta_0(\mu)\mathcal{Z})}\omega^2 d\omega d\mu$$
$$+\frac{\mathbf{e}_{\theta_0}}{(2\pi)^3}\int \frac{\sqrt{I_0(\mu)}\mu}{\rho_0}\left[\mathbf{K}^-_{\mathbf{x}}(\omega,\mu).\overline{\hat{\mathbf{f}}_{\mathbf{x}}}(\omega)+K^-_z(\omega,\mu)\overline{\hat{f}_z}(\omega)\right]e^{i\omega(\mu\mathcal{R}-\mathcal{T}-\zeta_0(\mu)\mathcal{Z})}\omega^2 d\omega d\mu$$

where

$$p^{hom}_{TR,\mathbf{x},z}(t) = -\frac{\hat{g}_2}{(4\pi)^2\rho_0^2c_0^2}\frac{(\mathbf{x}.\mathbf{x}_s+zz_s)}{\sqrt{r_s^2+z_s^2}^3\sqrt{|\mathbf{x}|^2+z^2}^3}\left[\mathbf{x}_s.\mathbf{f}''_{\mathbf{x}}(t)+z_sf''_z(t)\right]$$
$$\mathbf{v}^{hom}_{TR,\mathbf{x},z}(t) = -\frac{\hat{g}_2}{(4\pi)^2\rho_0c_0^3}\frac{(\mathbf{x}.\mathbf{x}_s+zz_s)\mathbf{x}}{\sqrt{r_s^2+z_s^2}^3\sqrt{|\mathbf{x}|^2+z^2}^3}\left[\mathbf{x}_s.\mathbf{f}''_{\mathbf{x}}(t)+z_sf''_z(t)\right]$$

The proof of the theorem follows the same line as the one of Theorem 3.1. In Section 4.3-4.4 we have derived the asymptotics of the expected value of the refocused pulse on the ring. To get the deterministic nature of the limit, it remains to compute the variance of the refocused field. It involves the computation of the forth moments of the generalized reflection and transmission coefficients. This is done again by using the final part of Appendix A.2.

5. Source Identification. In this section we indicate briefly how the results derived above are useful in solving the inverse source problem. We assume that we are in the configuration shown in figure 1.1. The source S emits a short pulse from an unknown location (x_s, z_s) at an unknown time t_s. Our objective is to identify these unknowns and the shape of the pulse assuming that we observe the signal that emerges at the surface at a receiver with a small spatial extent. Such a problem can be encountered in various contexts, such as geophysics [20] or oceanography [18]. The small aperture of the receiver in our configuration makes the identification of the source location challenging by standard methods. The known position of the receiver is chosen as the origin. We assume that the medium is randomly layered on a fine scale and that we know the particular realization "seen" by the wave. Our strategy is to perform a synthetic time reversal experiment meaning that we numerically solve the wave equation and compute the time reversed wave field described in the paper. In the regime of our asymptotic analysis the time reversed wave will exhibit a propagating spherical front wave and, at a precise time, an additional ring located at the depth of

the source and passing through the source point. This is precisely stated in Theorem 4.1. Note that the repropagated front wave can be computed by simply observing the first arrival at the receiver but it does not contain any information on the source location and time of emission. In contrast the use of the incoherent coda of the wave and time reversal techniques lead to an information about the depth of the source, its lateral distance from the mirror, and its emission time. The shape of the source pulse can then be reconstructed precisely by using the shape of the first arrival and a deconvolution process through the ODA kernel (A.7) described in Appendix A.5. Furthermore this identification can also be performed with the presence of additional noisy sources emitting at the surface. By the results of Section 4.5 the additional sources only produce refocused fields at the surface. The refocused ring is therefore produced only by the source inside the domain.

If only the statistical properties of the medium are known, but not the particular realization, the strategy would be to estimate the kernel from the measure of the wave emerging at the receiver and the computation of the local autocorrelation function of the signal [1]. This is a difficult problem which is a topic of future research. In other contexts such as underwater acoustics [14] the medium is not known but time reversal can be performed physically. The refocusing properties proved in this paper in an ideal layered setting can be used for telecommunication purposes.

6. Numerical Illustration. In this section we present a two dimensional numerical illustration of the theory developed in this paper. Time reversal refocusing is a phenomenon that takes place in different wave applications. Hence to illustrate its range of applicability we perform numerical experiments using a shallow water model.

The linear two dimensional shallow water equations [23] are given as

$$U_t = -g\eta_x + f_x \qquad V_t = -g\eta_y + f_y \tag{6.1}$$

$$\eta_t + [hU]_x + [hV]_y = 0, \tag{6.2}$$

where $U(x,y,t)$ and $V(x,y,t)$ are vertically z-averaged velocities. The free surface wave elevation is denoted by $\eta(x,y,t)$. This term represents the excess pressure about the undisturbed free surface $z \equiv 0$. The randomly layered medium is represented by the disordered bottom topography through $h(x,y)$. By using the flux vector $\psi = (\psi^u, \psi^v)^T \equiv (hU, hV)^T$ the correspondence between the shallow water and the acoustic model is more easily established:

$$\frac{\partial \psi}{\partial t} - gh\nabla\eta = 0, \tag{6.3}$$

$$\frac{\partial \eta}{\partial t} + \nabla \cdot \psi = 0. \tag{6.4}$$

The simulations refer to model (6.1,6.2). Details of the Lagrangian numerical scheme are provided in Casulli & Cheng [6]. We have adapted their code in order to have the data imposed through the velocity forcing terms. The setup for the numerical experiments is given in the schematic Fig. 6.1.

The random medium slab is located at $x > 0$. The source location is at $(x_S, y_S) = (10, 0)$ and we place two time reversal (point) mirrors at $(x_{M1}, y_{M1}) = (0, 4)$ and $(x_{M2}, y_{M2}) = (0, -4)$ corresponding to the surface location of the acoustic slab, here given by $x \equiv 0$. The velocity sources are such that both f_x and f_y have a Gaussian $f(t) = \exp(-(t - t_s)^2/0.02)$ profile of duration approximately equal to 1/3 time

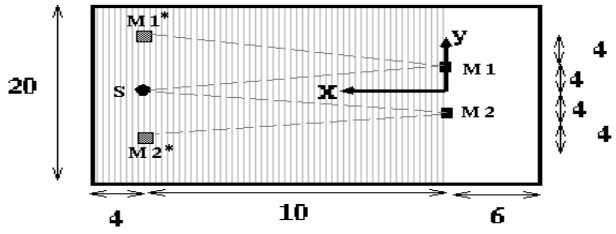

FIG. 6.1. *Schematic setup for the randomly layered topography. The source point* **S** *is at* $(x_S, y_S) = (10, 0)$ *corresponding to nodes (1600,1000). The shaded area represents the randomly layered medium.*

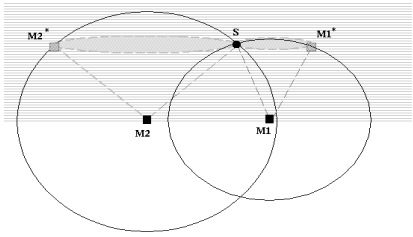

FIG. 6.2. *Schematic graph for the wave fronts (centered at the mirrors* $M1$ *and* $M2$*) together with the refocusing rings (dashed curves). Each ring is at the base of a three dimensional cone defined by the corresponding triplet* (M, M^*, S)*. The shaded area highlights the* xz *circle/ring intersecting the* xy *plane.*

units. The randomly layered topography has a correlation length of 0.1 with 40% fluctuations about the undisturbed depth. A nearly circular, pulse shaped, wave front propagates over the random medium and time histories (for the velocity fields) are recorded at mirror $M1$ and mirror $M2$, as displayed in Fig. 6.3. We observe the wave front arriving, at approximately $t = 10.8$ followed by a fluctuating coda. We time reverse the signals recorded within the time interval [10.8 18.8]. In the time reversal experiment these are the corresponding f-profiles, now at two Dirac source locations, each corresponding to a point mirror. We repeat the numerical solution procedure and two pulse shaped fronts propagate towards the source location. In all numerical experiments we use a 2000 by 2000 spatial grid with $\Delta x = \Delta y = 0.01$. The time stepping parameter is $\Delta t = 0.0005$. These were chosen due to accuracy and not for stability reasons [6]. We have used reflecting boundary conditions. As can be seen in some graphs presented below, they do not interfere with our region of interest, during the time interval of our study. Reflected waves, from the side walls, will always be away from our region of interest.

As mentioned before the time reversed signals, indicated in Fig. 6.3, are back-propagated from the two mirrors. The theory predicts two refocusing rings since we have two mirrors. A schematic picture for the rings' configuration is given in Fig. 6.2. In our particular example both rings will have the same radius since the mirrors are positioned symmetrically with respect to the source. By no means this is a special configuration. As indicated by a grey disk in Fig. 6.2, in a two dimensional problem

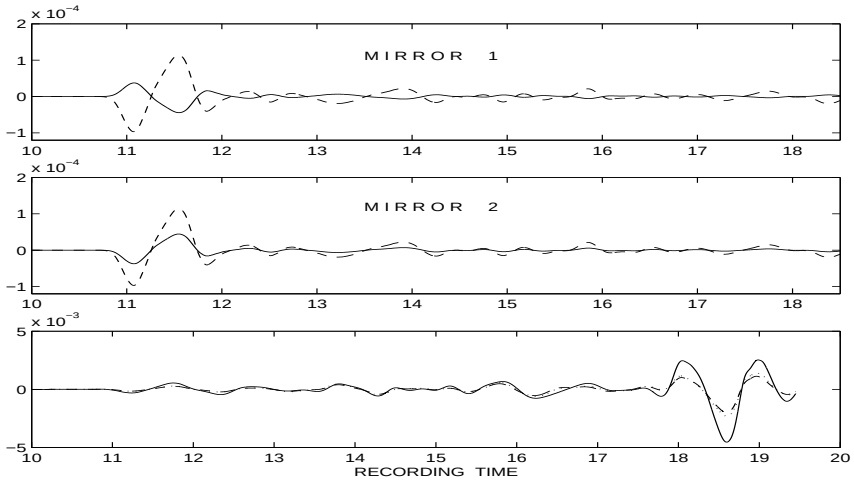

FIG. 6.3. *(Top and Middle) Recorded signals at the two mirrors: dashed line represents U while the solid line represents V. (Bottom) Time history for the wave elevation η at the source location (solid line), at the top image point $M1^*$ (dashed line) and the bottom image point $M2^*$ (dotted line).*

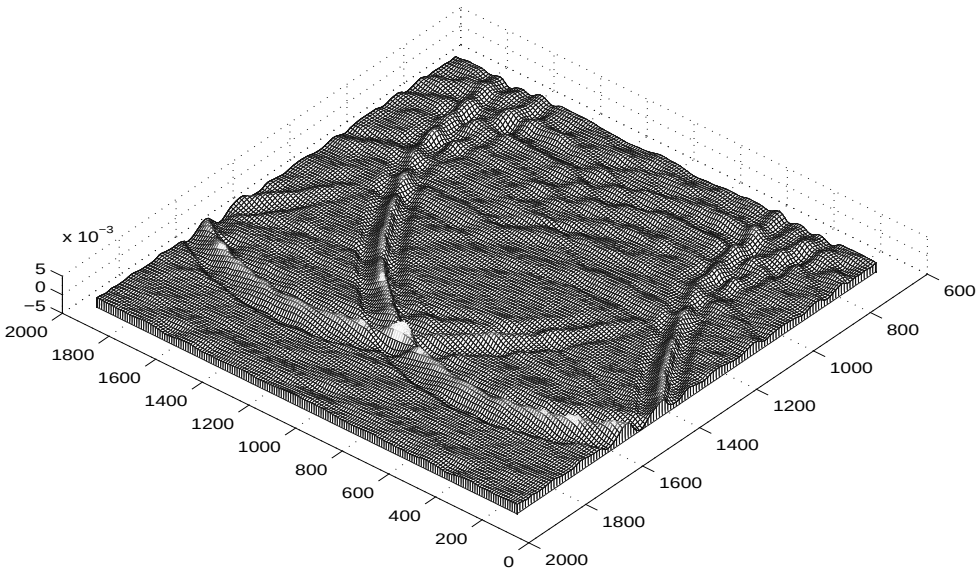

FIG. 6.4. *Numerical simulation in a random medium. Refocusing observed at three bright spots: source point (spot at the middle) and two image points, namely at nodes (1600,1800) and (1600,200). Snapshot at the critical time $t_c = 18.80$.*

each refocusing ring will be identified by two points, namely the intersection of the ring with the xy plane. The rings, corresponding to each mirror, will coincide (and add up) at the source point but will also define *image points* corresponding to the other point of each ring's cross section with the xy plane. We will label these image points as $M1^*$ and $M2^*$ in connection with the notation of the corresponding point mirror. In Fig. 6.1 and Fig. 6.2 they are indicated by two grey squares near the source point. At the bottom graph of Fig. 6.3 we have the time history at the

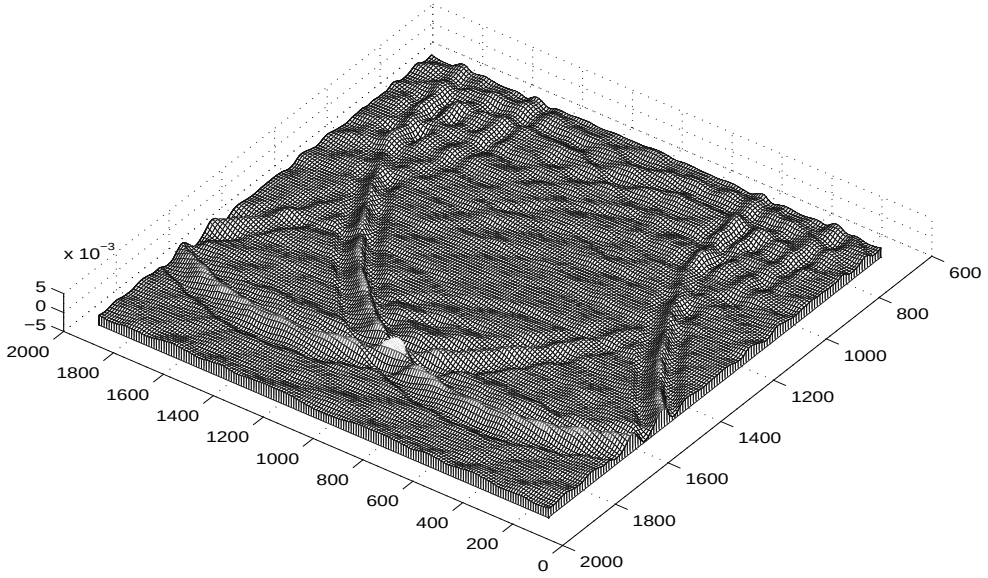

FIG. 6.5. *Numerical simulation in a random medium. Snapshot at a later time* $t = 19.80$. *Image points have vanished.*

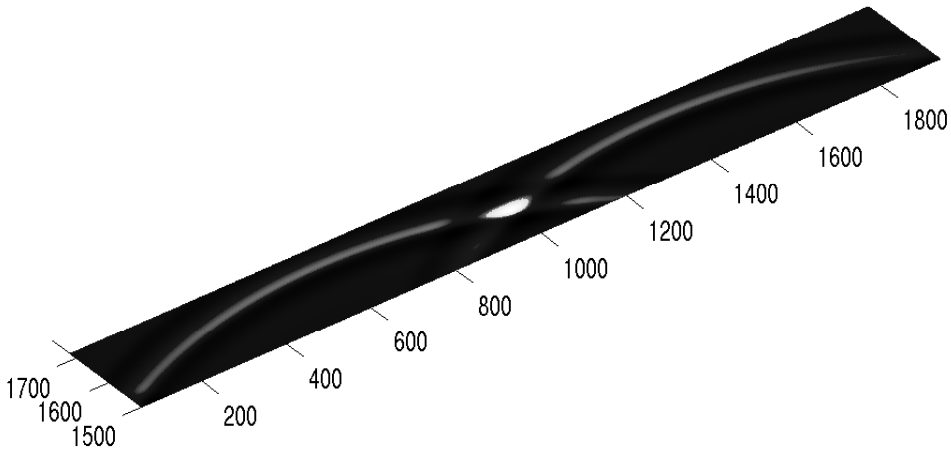

FIG. 6.6. *Numerical simulation in a homogeneous medium.*

source location and also at the image points $M1^*$ and $M2^*$. As expected the front is the second derivative of a Gaussian (namely of $f(t)$). For better visualization of refocusing, at the front's largest (absolute) value, from now on we will graph minus the value of the wave elevation. We start with a three-dimensional graph (Fig. 6.4; a snapshot at $t = 18.80$ for the wave elevation) corresponding to the same experiment which generated the traces in Fig. 6.3. Along the wave front we see three bright spots corresponding to the source location (1600,1000) and the two image points (1600,200) and (1600,1800). We now compare it with a slightly later snapshot (Fig. 6.5) and the bright image spots have vanished. The image spots are very difficult to capture

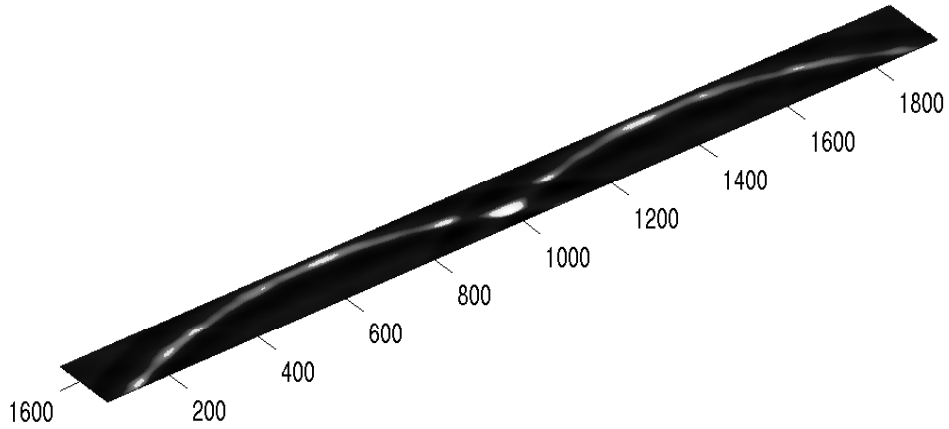

FIG. 6.7. *Numerical simulation in a random medium. Snapshot (at* $t = 18.25$*) before the critical time (*$t_c = 18.80$*).*

numerically since the coda has to be very long in order to contain a nontrivial amount of energy and also because its "life-span" is very short in time over a very small region of the computational domain. In order to provide stronger evidence of the facts here describe we present high-contrast (HC) pictures for the front near the source location.

In the first HC picture we consider time-reversal in a homogeneous medium. The time reversed data has been emited from the two point mirrors and in Fig. 6.6 the two fronts have reached the source location. Obviously there are no image points, since we are in a homogenous medium. The central bright spot (Fig. 6.6) is due to the superposition of the two fronts. Note that in this case it is impossible to locate the source. The bright spot propagates (unchanged) along the x-axis. Nevertheless, as pointed out in this paper, the source can be located in the presence of randomness, due to the image points.

To illustrate this note that in Fig. 6.7 we have the wavefront right before refocusing takes place. In Fig. 6.8, at the critical time, we now observe a larger bright spot at the source (refocusing) point and also two smaller bright spots, also along the leading front. In particular the numerical refocusing was better at (1600,200) giving a brighter image point. These are the image points mentioned above, and represent the other points where the refocusing rings intersect the xy plane. To further highlight this phenomenon we now observe the wavefront at a (slightly) later time in Fig. 6.9. We see that the middle spot is slightly weaker while the image points have disappeared. This clearly indicates refocusing in time and space: beyond the critical time the refocusing ring does not exist anymore. Hence the presence of the image points indicate the precise time where the central bright spot is over the source.

Appendix A. Statistical properties of the reflection and transmission coefficients.

A.1. Moments at different slowness vectors. The values of the moments of the transmission coefficient at different slowness vectors is required in Section 4.4.2. Let us consider $z_0 < z_1, z_1'$, a central frequency ω, $n + n'$ small relative frequency shifts h_1,...,h_n, h_1',... $h_{n'}'$ and $n + n'$ different slowness vector moduli $\kappa_1 \neq ... \neq \kappa_n \neq$

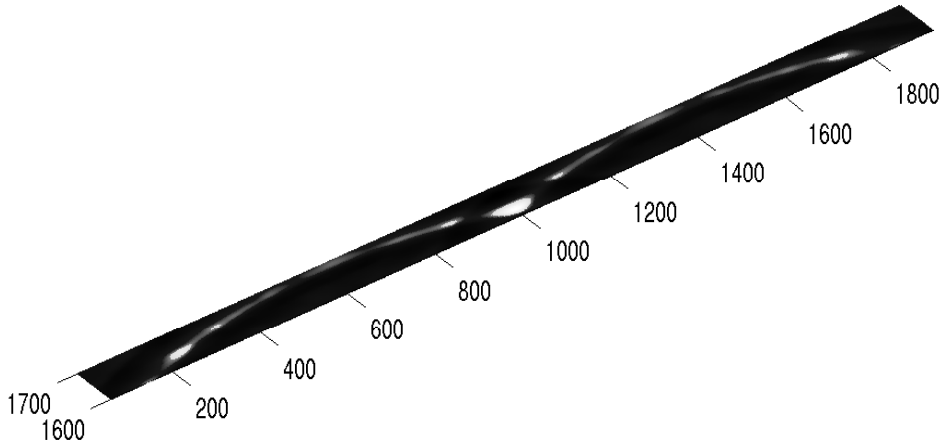

FIG. 6.8. *Numerical simulation in a random medium. Refocusing observed at three bright spots: source point (spot at the middle) and two image points. Snapshot at* $t_c = 18.80$

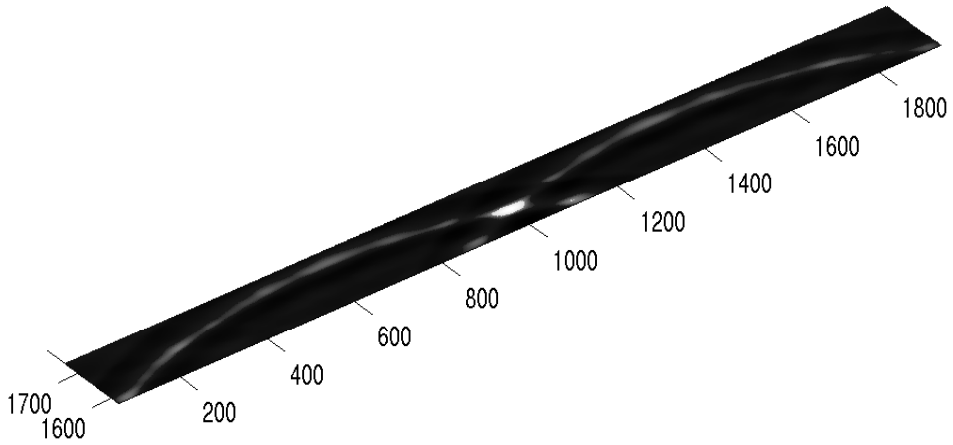

FIG. 6.9. *Numerical simulation in a random medium. Snapshot beyond the critical time (*$t = 18.95$*).*

$\kappa'_1 \neq ... \neq \kappa'_{n'}$. The computation of the limits of the following moments

$$\lim_{\varepsilon \to 0} \mathbb{E}\left[\prod_{j=1}^{n} T(\omega + \varepsilon h_j, \kappa_j, z_0, z_1) \prod_{j=1}^{n'} \overline{T}(\omega + \varepsilon h'_j, \kappa'_j, z_0, z'_1)\right]$$

has been carried out in [7]. It is found that the limits are

$$\mathbb{E}\left[\prod_{j=1}^{n} T_{\text{eff}}(\omega, \kappa_1, z_0, z_1) \prod_{j=1}^{n'} \overline{T_{\text{eff}}}(\omega, \kappa'_j, z_0, z'_1)\right]$$

where

$$T_{\rm eff}(\omega,\kappa,z_0,z)=\exp\left(i\sqrt{\gamma(\omega,\kappa)}(B_z-B_{z_0})-\frac{\gamma(\omega,\kappa)(z-z_0)}{2}\right)$$

B is a standard one-dimensional Brownian motion. The same computation carried out with the reflection coefficient leads to the limit

$$\lim_{\varepsilon\to 0}\mathbb{E}\left[\prod_{j=1}^{n}R(\omega+\varepsilon h_j,\kappa_j,z_0,z_1)\prod_{j=1}^{n'}\overline{R}(\omega+\varepsilon h'_j,\kappa'_j,z_0,z'_1)\right]=0$$

A.2. Autocorrelation function of the reflection coefficient at two nearby slowness vectors and frequencies. Taking the expectation of the integral representation (3.1) of the signal shows that the autocorrelation function of the reflection coefficient at two nearby frequencies and slowness vectors plays a crucial role. As shown in [1, 5] we have, for $z_0\le z$,

$$\begin{aligned}&\mathbb{E}\left[R^n(\omega-\frac{\varepsilon h}{2},\kappa-\frac{\varepsilon\lambda}{2},z_0,z)\overline{R}^m(\omega+\frac{\varepsilon h}{2},\kappa+\frac{\varepsilon\lambda}{2},z_0,z)\right]\\ &\xrightarrow{\varepsilon\to 0}\begin{cases}\displaystyle\int W_n(\tau,\omega,\kappa,z_0,z)e^{i\tau[c_0^2\omega\kappa\lambda-h(1-c_0^2\kappa^2)]}d\tau & \text{if } m=n\\ 0 & \text{otherwise}\end{cases}\end{aligned}$$

where the quantity W_n is obtained through the following system of transport equations

$$\begin{aligned}&\frac{\partial W_n}{\partial z}+2n\frac{\partial W_n}{\partial\tau}=\gamma(\omega,\kappa)n^2\left(W_{n+1}+W_{n-1}-2W_n\right)\\ &W_n(\tau,\omega,\kappa,z_0,z=z_0)=\mathbf{1}_0(n)\delta(\tau)\end{aligned}$$

that has a probabilistic interpretation. In order to describe this interpretation we introduce the jump Markov process $(N(z))_{z\ge z_0}$ with state space $\mathbb{N}$ and infinitesimal generator

$$\mathcal{L}\phi(N)=\gamma(\omega,\kappa)N^2\left(\phi(N+1)+\phi(N-1)-2\phi(N)\right),$$

where

$$\gamma(\omega,\kappa)=\frac{\gamma_0\omega^2}{2c_0^4\zeta_0(\kappa)^2},\qquad \gamma_0=\int_0^\infty\mathbb{E}[\nu(0)\nu(z)]dz \tag{A.1}$$

is the integrated correlation of the medium. Following [1] W_n can be written as the expectation of a functional of this jump process

$$W_n(\tau,\omega,\kappa,z_0,z)=\mathbf{E}\left[\delta\left(\tau-\frac{2}{c_0^2\zeta_0(\kappa)}\int_{z_0}^{z}N(u)du\right)\mathbf{1}_{\{N(z)=0\}}\,\middle|\,N(z_0)=n\right] \tag{A.2}$$

where $\mathbf{E}$ stands for the expectation over the distribution of the jump process. The case with a large slab ($z_0\to-\infty$) leads to explicit formulas for the autocorrelation function of the reflection coefficient. Indeed the hyperbolicity of the equations makes the reflected quantities of interest, for a finite observation time, independent of z_0, z for $z-z_0$ large enough. This leads to explicit formulas for the power spectral density

W_n. Applying results from [1] we get that the function W_n converges as $z_0 \to -\infty$ to the limit

$$W_n(\tau,\omega,\kappa,z_0,z) \overset{z_0\to-\infty}{\longrightarrow} Q_n\left(\frac{c_0^2\zeta_0(\kappa)}{2}\tau\right)\frac{c_0^2\zeta_0(\kappa)}{2}$$

where

$$Q_n(u) = \frac{\partial}{\partial u}\left[\left(\frac{\gamma(\omega,\kappa)}{1+\gamma(\omega,\kappa)u}\right)^n \mathbf{1}_{[0,\infty)}(u)\right]. \tag{A.3}$$

Accordingly, the limit value of the expectation of the autocorrelation function of the reflection coefficient is

$$\begin{aligned}&\mathbb{E}\left[R(\omega-\frac{\varepsilon h}{2},\kappa-\frac{\varepsilon\lambda}{2},z_0,z)\overline{R}(\omega+\frac{\varepsilon h}{2},\kappa+\frac{\varepsilon\lambda}{2},z_0,z)\right]\\ &\overset{\varepsilon\to0}{\longrightarrow}\int_0^\infty Q_1\left(\frac{c_0^2\zeta_0(\kappa)}{2}\tau\right)\frac{c_0^2\zeta_0(\kappa)}{2}e^{i\tau[\omega\lambda c_0^2\kappa-hc_0^2\zeta_0(\kappa)^2]}d\tau\end{aligned} \tag{A.4}$$

Denoting $U_j^\varepsilon = R(\omega_j-\frac{\varepsilon h_j}{2},\mu_j-\frac{\varepsilon\lambda_j}{2},0)\overline{R}(\omega_j+\frac{\varepsilon h_j}{2},\mu_j+\frac{\varepsilon\lambda_j}{2},0)$, it is shown in [5] that for two distinct frequencies $\omega_1\neq\omega_2$ or for distinct $\mu_1\neq\mu_2$ one has

$$|\mathbb{E}\left[U_1^\varepsilon U_2^\varepsilon\right]-\mathbb{E}\left[U_1^\varepsilon\right]\mathbb{E}\left[U_2^\varepsilon\right]| \overset{\varepsilon\to0}{\longrightarrow} 0. \tag{A.5}$$

This decorrelation property is used in this paper to deduce the self-averaging property of the refocused pulse. We also use the fact that the reflection coefficients at distinct frequencies decorrelate as $\varepsilon\to0$ and that their means average to zero to show that the P_2 and P_4 terms of the velocity field are vanishing as $\varepsilon\to0$.

A.3. Autocorrelation function of the transmission coefficient at two nearby slowness vectors and frequencies. Cross-moments of transmission and reflection coefficients are required in Section 4. Extending once again the results contained in [1], we get that

$$\begin{aligned}&\mathbb{E}\left[R^nT(\omega-\frac{\varepsilon h}{2},\kappa-\frac{\varepsilon\lambda}{2},z_0,z)\overline{R^mT}(\omega+\frac{\varepsilon h}{2},\kappa+\frac{\varepsilon\lambda}{2},z_0,z)\right]\\ &\overset{\varepsilon\to0}{\longrightarrow}\begin{cases}\displaystyle\int_0\widetilde{W}_n(\tau,\omega,\kappa,z_0,z)e^{i\tau[c_0^2\omega\kappa\lambda-h(1-c_0^2\kappa^2)]}d\tau & \text{if } m=n\\ 0 & \text{otherwise}\end{cases}\end{aligned}$$

where the quantity $\widetilde{W}_n$ is obtained through the following system of transport equations

$$\begin{aligned}&\frac{\partial\widetilde{W}_n}{\partial z}+2n\frac{\partial\widetilde{W}_n}{\partial\tau}=\gamma(\omega,\kappa)\left((n+1)^2\widetilde{W}_{n+1}+n^2\widetilde{W}_{n-1}-(n^2+(n+1)^2)\widetilde{W}_n\right)\\ &\widetilde{W}_n(\tau,\omega,\kappa,z_0,z=z_0)=\mathbf{1}_0(n)\delta(\tau)\end{aligned}$$

$\widetilde{W}_n$ has the following probabilistic interpretation

$$\widetilde{W}_n(\tau,\omega,\kappa,z_0,z)=\mathbf{E}\left[\delta\left(\tau-\frac{2}{c_0^2\zeta_0(\kappa)}\int_{z_0}^z\widetilde{N}(u)du\right)\mathbf{1}_{\left\{\widetilde{N}(z)=0\right\}}\middle|\,\widetilde{N}(z_0)=n\right] \tag{A.6}$$

in terms of the jump Markov processes $\widetilde{N}$ with infinitesimal generator

$$\widetilde{\mathcal{L}}\phi(\widetilde{N})=\gamma(\omega,\kappa)\left[(\widetilde{N}+1)^2\phi(\widetilde{N}+1)+\widetilde{N}^2\phi(\widetilde{N}-1)-((\widetilde{N}+1)^2+\widetilde{N}^2)\phi(\widetilde{N})\right]$$

and $\gamma(\omega,\mu)$ is defined by Eq. (A.1).

A.4. Shift properties. Straightforward manipulations based on shifts of the governing equations show that

$$(R(\omega,\kappa,z,z_1),T(\omega,\kappa,z,z_1),\nu(z))_{z_0\le z\le z_1}$$

and

$$\Big(R(\omega,\kappa,z-z_1,0)e^{2i\frac{\omega\zeta_0(\kappa)z_1}{\varepsilon}},T(\omega,\kappa,z-z_1,0),\nu(z-z_1)\Big)_{z_0\le z\le z_1}$$

have the same distribution. Similarly,

$$(R(\omega,\kappa,z,0),T(\omega,\kappa,z,0),\nu(z))_{z_0\le z\le 0}$$

and

$$\Big(\tilde R(\omega,\kappa,z,0)e^{-2i\frac{\omega\zeta_0(\kappa)z_0}{\varepsilon}},\tilde T(\omega,\kappa,z,0),\nu(z_0-z)\Big)_{z_0\le z\le 0}$$

have the same distribution.

A.5. The coherent pulse front in the random case. In this section we compute the expression of the coherent front pulse that can be recorded at the surface. The source is assumed to be inside the medium, i.e. $z_s<0$, so the front pulse emitted by the source propagates through the random medium and its propagation is actually governed by the well known O'Doherty Anstey (ODA) theory. In Section 4.1 we computed this front pulse (Eq. (4.1)) as well as the time reversal of this front pulse (Eq. (4.2)) in homogeneous medium. We now revisit these results in presence of randomness. In this case the front pulse is modified in two ways. First its shape spreads out in a deterministic way due to multiple scattering. This spreading can be described in terms of the convolution ODA kernel K_{ODA} [13]. Second the wave itself is not anymore deterministic but a random time shift can be observed and described in terms of a standard Brownian motion B_z. To sum-up, the pulse front that can be recorded at the surface is

$$\begin{aligned}u_s(t,\mathbf{x},z=0)=\frac{1}{(2\pi)^3\varepsilon^2}\int\frac{1}{2\sqrt{I_0(\kappa)}}e^{-i\omega\frac{t-t_s-\boldsymbol{\kappa}.(\mathbf{x}-\mathbf{x}_s)+\zeta_0(\kappa)z_s}{\varepsilon}}\\ \times\hat K_{ODA}(\omega,\boldsymbol{\kappa})S_a(\omega,\boldsymbol{\kappa})\omega^2d\omega d\boldsymbol{\kappa}\\ \hat K_{ODA}(\omega,\boldsymbol{\kappa})=\exp\left(i\sqrt{\gamma(\omega,\kappa)}B_{z_s}+\frac{\gamma(\omega,\kappa)z_s}{2}\right)\end{aligned}$$

If the field is observed just above the source, that is to say $\mathbf{x}=\mathbf{x}_s$, then the rapid phase reduces to $\omega(t_s-t-\zeta_0(\kappa)z_s)$ and a stationary phase argument shows that the leading order contribution is associated with the stationary point $\kappa=0$. The longitudinal field then reads

$$u_s(t,\mathbf{x}_s,z=0)=\frac{1}{2(2\pi)^2z_s\rho_0c_0^2}\int e^{-i\omega\frac{t-t_s+z_s}{\varepsilon}}e^{\left[i\omega\frac{\sqrt{\gamma_0}}{\sqrt{2}c_0}B_{z_s}+\frac{\gamma_0\omega^2z_s}{4c_0^2}\right]}(\frac{i\omega}{\varepsilon})\hat f(\omega)d\omega$$

In the case $\gamma_0=0$, this reduces exactly to (4.1) with $z=0$. If we denote the longitudinal velocity in homogeneous medium by u_s^{hom}, then in presence of randomness $\gamma_0>0$ the longitudinal velocity field can be written as the convolution with a Gaussian kernel

$$u_s(t,\mathbf{x}_s,z=0)=\left[u_s^{hom}(.,\mathbf{r}=(\mathbf{x}_s,0))*\mathcal{N}\right](t-\frac{\sqrt{\gamma_0}}{\sqrt{2}c_0}B_{z_s}),$$

where

$$\mathcal{N}(t) = \frac{c_0}{\sqrt{\gamma_0|z_s|\pi}} \exp\left(-\frac{c_0^2 t^2}{\gamma_0|z_s|}\right)$$

If we observe the velocity field at a different point at the surface $\mathbf{x} \neq \mathbf{x}_s$, then the qualitative picture remains unchanged in the sense that we still observe the unperturbed front u_s^{hom} randomly time-delayed and convoluted with a deterministic Gaussian kernel. The only difference is that this kernel is obtained by evaluating the ODA kernel K_{ODA} at a non-zero stationary slowness vector $\boldsymbol{\kappa}$ that results from the stationary phase argument. The result is that the longitudinal velocity field can be written as the convolution of the unperturbed front with a specific Gaussian kernel

$$u_s(t, \mathbf{x}, z = 0) = \left[u_s^{hom}(., \mathbf{r} = (\mathbf{x}, 0)) * \mathcal{N}_{\mathbf{x}}\right](t - \frac{\sqrt{\gamma_{\mathbf{x}}}}{\sqrt{2}c_0} B_{z_s}),$$

where

$$\mathcal{N}_{\mathbf{x}}(t) = \frac{c_0}{\sqrt{\gamma_{\mathbf{x}}|z_s|\pi}} \exp\left(-\frac{c_0^2 t^2}{\gamma_{\mathbf{x}}|z_s|}\right), \qquad \gamma_{\mathbf{x}} = \gamma_0 \frac{\sqrt{|\mathbf{x} - \mathbf{x}_s|^2 + z_s^2}}{|z_s|} \tag{A.7}$$

REFERENCES

[1] M. Asch, W. Kohler, G. Papanicolaou, M. Postel, and B. White, Frequency content of randomly scattered signals, SIAM Rev. **33** (1991) 519-625.

[2] G. Bal, G. Papanicolaou, and L. Ryzhik, Self-averaging in time reversal for the parabolic wave equation, Stochastics and Dynamics **2** (2002) 507-531.

[3] L. Berlyand and R. Burridge, The accuracy of the O'Doherty-Anstey approximation for wave propagating in highly disordered stratified media, Wave Motion **21** (1995) 357-373.

[4] P. Blomgren, G. Papanicolaou, and H. Zhao, Super-resolution in time-reversal acoustics, J. Acoust. Soc. Am. **111** (2002) 230-248.

[5] R. Burridge, G. Papanicolaou, and B. White, Statistics for pulse reflection from a randomly layered medium, SIAM J. Appl. Math. **47** (1987) 146-168.

[6] V. Casulli and R. Cheng, Semi-implicit finite difference methods for three-dimensional shallow water flow, Int. J. Num. Meth. Fluids, 15, (1992) 629-648.

[7] J. Chillan and J.-P. Fouque, Pressure fields generated by acoustical pulses propagating in randomly layered media, SIAM J. Appl. Math. **58** (1998) 1532-1546.

[8] J.-F. Clouet and J.-P. Fouque, Spreading of a pulse traveling in random media, Annals of Applied Probability **4** (1994) 1083-1097.

[9] J.-F. Clouet and J.-P. Fouque, A time-reversal method for an acoustical pulse propagating in randomly layered media, Wave Motion **25** (1997) 361-368.

[10] A. Derode, A. Tourin, J. de Rosny, M. Tanter, S. Yon, and M. Fink, Taking advantage of multiple scattering to communicate with time reversal antennas, Phys. Rev. Lett. **90** (2003) 014301.

[11] M. Fink, Time reversed acoustics, Scientific American (November 1999) 91-97.

[12] M. Fink, G. Montaldo, and M. Tanter, Time reversal acoustics in biomedical engineering, Annual Review of Biomedical Engineering **5** (2003) 465-497.

[13] J.-P. Fouque and K. Sølna, Time-reversal aperture enhancement, SIAM Multiscale Modeling and Simulation **1** (2003) 239-259.

[14] W. A. Kuperman, W. S. Hodgkiss, H. C. Song, T. Akal, C. Ferla, and D. R. Jackson, Phase conjugation in the ocean, experimental demonstration of an acoustic time-reversal mirror, J. Acoust. Soc. Am. **103** (1998) 25-40.

[15] P. Lewicki, R. Burridge, and G. Papanicolaou, Pulse stabilization in a strongly heterogeneous medium, Wave Motion **20** (1994) 177-195.

[16] G. Papanicolaou, Wave propagation in a one-dimensional random medium, SIAM J. Appl. Math. **21** (1971) 13-18.

[17] G. Papanicolaou, L. Ryzhik and K. Sølna, Statistical stability in time reversal, to appear in SIAM J. Appl. Math. (2003).

[18] C. Pires and M. A. Miranda, Tsunami waveform inversion by adjoint methods, J. Geophys. Res. **106** (2001) 19733-19796.
[19] C. Prada, E. Kerbrat, D. Cassereau, and M. Fink, Time reversal techniques in ultrasonic nondestructive testing of scattering media, Inverse Problems **18** (2002) 1761-1773.
[20] R. Snieder, Imaging and averaging in complex media, in Diffusive wave in complex media, J.-P. Fouque, ed., NATO Science Series C, Vol 531, Kluwer, 1999, pp. 405-454.
[21] K. Sølna, Focusing of time-reversed reflections, Waves in Random Media **12** (2002) 365-385.
[22] K. Sølna and G. Papanicolaou, Ray theory for a locally layered medium, Waves in Random Media **10** (2000) 151-198.
[23] G.B. Whitham, Linear and Nonlinear Waves, Wiley, New York, (1974).
[24] L. Mandel and E. Wolf, Optical coherence and quantum optics, Cambridge University Press, Cambridge (1995).